Master's thesis

NTNU
Norwegian University of Science and Technology
Faculty of Natural Sciences
Department of Chemical Engineering

Øyvind Vilfred Haugberg Lille-Mæhlum

Modelling Solvent Degradation in Amine-based Post-combustion Carbon Capture

Master's thesis in Chemical Engineering and Biotechnology
Supervisor: Hanna Knuutila
Co-supervisor: Lucas Braakhuis

June 2021

NTNU
Norwegian University of
Science and Technology

Øyvind Vilfred Haugberg Lille-Mæhlum

Modelling Solvent Degradation in Amine-based Post-combustion Carbon Capture

Master's thesis in Chemical Engineering and Biotechnology
Supervisor: Hanna Knuutila
Co-supervisor: Lucas Braakhuis
June 2021

Norwegian University of Science and Technology
Faculty of Natural Sciences
Department of Chemical Engineering

NTNU
Norwegian University of
Science and Technology

Preface

This thesis was written during the spring of 2021 as the final fulfilment of the five-year master's degree program of Chemical Engineering and Biotechnology at the Norwegian University of Science and Technology (NTNU).

I declare that this is an independent work according to the exam regulations of the Norwegian University of Science and Technology.

Trondheim, June 2021

Øyvind Vilfred Haugberg Lille-Mæhlum

Acknowledgement

I wish to express my deep and sincere gratitude to my supervisors Hanna Knuutila and Lucas Braakhuis. I thank them for our interesting weekly meetings where they have challenged me and guided me through this work.

I would also like to thank the employees of SINTEF, Solrun Johanne Vevelstad, Geir Haugen, Andreas Grimstvedt and Aslak Einbu for providing data and for the valuable discussions regarding the campaign in the solvent degradation rig.

Abstract

Amine-based Post-combustion Carbon Capture (PCC) is a promising way of reducing the constantly increasing anthropogenic CO_2 emissions. In this process, there are two significant problems. The first problem is solvent degradation, and the second problem is the considerable energy consumption this process requires. Further research should be done to fully understand and reduce solvent degradation while at the same time minimising the energy consumption of the process.

In this master thesis, two degradation models were used to predict solvent degradation of Monoethanolamine (MEA). These models were evaluated on a lab-scale experiment, a pilot plant, and two industrial cases.

The models were first validated by comparing the observed degradation seen at lab-scale experiment and the pilot plant. The advanced model predicts an MEA loss which was comparable to the lab-scale experiment. The simplified model fits best for the pilot plant. The prediction of the degradation compounds HEI, formic acid, HEEDA, and HEIA seem to fit relatively close to what was found at the lab-scale experiment.

By comparing flue gases emitted by a coal and a natural gas-based power plant, solvent degradation was found to be most significant for coal. The optimal liquid-to-gas ratio concerning energy consumption was found to be 2.6 for coal and 1.1 for natural gas. The specific MEA consumptions from typical 400 MW coal and natural gas-based power plants were found to be 0.35 and 0.25 kg MEA/t_{CO_2}, respectively, by the advanced model. The simplified model predicted the specific MEA consumption to be 0.55 and 0.37 kg MEA/t_{CO_2}, for coal and natural gas, respectively. Based on similar specific energy consumption in the two cases and based on the model's prediction on degradation, flue gases from natural gas might be most economical in terms of operating expenses in an amine-based post-combustion carbon capture plant.

Sammendrag

Aminbasert karbonfangst er en teknologi som kan redusere de stadig større menneskeligskapte CO_2-utslippene. Det er likevel to problemer med denne teknologien. For det første vil løsningsmiddelet som brukes for å reagere med CO_2 brytes ned. Det andre problemet er at prosessen krever store mengder energi. Videre forskning bør bli gjort for å forstå nedbrytningen av løsningsmiddelet mens man minimerer energibehovet i prosessen.

I denne masteroppgaven ble to modeller brukt for å estimere mengden av løsningsmiddelet Monoetanolamin (MEA) som blir nedbrutt i en eksperimentell rigg, i et pilotanlegg for karbonfangst og i to industrielle anlegg.

Modellene ble validert ved å sammenligne nedbrytningen som ble målt fra en eksperimentell rigg i labskala, og med nedbrytningen som ble målt ved et pilotanlegg. Det viser seg at den avanserte modellen var mest nøyaktig for riggen, mens den enkle modellen egnet seg best for pilotanlegget. Konsentrasjonene av komponentene som stammet fra nedbrytningen, HEI, maursyre, HEEDA og HEIA som den avanserte modellen estimerte var nokså nøyaktig sammenlignet med eksperimentet i riggen.

Fra sammenlikning mellom røykgass fra et kullkraftverk og et kraftverk basert på naturgass ble det funnet mest nedbrytning ved å rense røykgassen fra kullkraftverket. Det energimessig optimale forholdet mellom løsningsmiddelet og røykgassen ble funnet til 2,6 for kull og 1,1 for naturgass. Den avanserte modellen beregnet et MEA-konsum for et typisk 400 MW kullkraftverk til 0,35 kg MEA/t_{CO_2}, mens for naturgass var det 0,25 kg MEA/t_{CO_2}. Den enkle modellen beregnet 0,55 og 0,37 kg MEA/t_{CO_2} for henholdsvis kull og naturgass. Basert på de nokså like energibehovene kunne det fastslås at det er mest økonomisk gunstig å installere karbonfangstteknologi på kraftverk basert på naturgass.

TABLE OF CONTENTS

LIST OF TABLES

LIST OF FIGURES

List of Symbols

Symbol	Unit	Description
A	m^2	Cross section area
A_i		Pre-exponential factor
$C_{G,0}$	mol/L	Gas solubility in water
C_G	mol/L	Gas solubility in electrolyte solution
$\overline{Cp}$	kJ/kgK^{-1}	Specific heat capacity
E_a	J/mol	Activation energy
f_x	-	Reaction efficiency of component x
h_G	$m^3/kmol$	Gas-specific parameter
h_i	$m^3/kmol$	Ion-specific parameter
h_T	$m^3/kmolK^{-1}$	Temperature's effect of the gas specific parameter
$H_{vap,i}$	kJ/kg	Heat of water vapourisation
K_r		Reference reaction rate coefficient
k_T		Reaction rate coefficient
$\overline{m}$	kg/s	Average mass flow of solvent
$\dot{n}_{\mathrm{CO_2}}$	kg/s	Stripping molar flow rate
n_i	kg/s	Flow rate of component i
$n_{vap,i}$	kg/s	Molar flow rate of vaporised component i
p_i	Bar	Partial pressure of component i
Q_{Reb}	kW	Reboiler duty
R	8.314 $J/Kmol^{-1}$	Gas constant
R_T	mol/m^3s^{-1} & $mol/Lday^{-1}$	Rate of reaction, advanced thermal
$R_{x,i}$	$mol/Lday^{-1}$	Rate of reaction, advanced oxidative
$-r_{MEA,oxidative}$	mol/Ls^{-1}	Rate of reaction, simple oxidative
$-r_{MEA,thermal}$	mol/m^3s^{-1}	Rate of reaction, simple thermal
T	K	Temperature
$\dot{V}$	m^3/h	Flow rate in vapour phase
V	m^3 & L	Volume
α	$mol_{\mathrm{CO_2}}/mol_{MEA}$	Loading
$\Delta \mathrm{H}_i$	kJ/kg	Heat of CO_2 desorption
υ	[m/s]	Gas velocity

Abbreviations

Exp	Experimental
FOLU	Forestry and Other Land Use
GHG	Greenhouse Gases
HSS	Heat Stable Salts
IPCC	Intergovernmental Panel on Climate Change
L/G	Liquid-to-Gas
MEA	Monoethanolamine
MW	Molecular Weight
NTNU	Norwegian University of Science and Technology
PCC	Post-combustion Carbon Capture
$t_{\mathrm{CO_2}}$	Ton of Carbon Dioxide
Vol%	Volume Percent
Wt%	Weight Percent

Chemicals

Abbreviation	Name	Formula	Molecular weight	CAS
BHEOX	N1,N2-bis(2-hydroxyethyl)-ethanediamide	$C_6H_{12}N_2O_4$	176.17	1871-89-2
HEEDA	2-[(2-aminoethyl)amino]-ethanol	$C_4H_{12}N_2O$	104.15	111-41-1
HEF	N-(2-hydroxyethyl)-formamide	$C_3H_7NO_2$	89.05	693-06-1
HEGly	N-(2-hydroxyethyl)-glycine	$C_4H_9NO_3$	119.12	5835-28-9
HEI	1H-Imidazole-1-ethanol	$C_5H_8N_2O$	112	1615-14-1
HEIA	1-(2-hydroxyethyl)-2-imidazolidinone	$C_5H_{10}N_2O_2$	130.15	3699-54-5
HEPO	4-(2-hydroxyethyl)-2-piperazinone	$C_6H_{12}N_2O_2$	144.17	23936-04-1
OZD	2-oxazolidinone	$C_3H_5NO_2$	87.08	497-25-6
MEA	Monoethanolamine	C_2H_7NO	61.08	141-43-5
	Ammonia	NH_3	17.03	7664-41-7
	Formaldehyde	CH_2O	30.03	50-00-0
	Formic acid	CH_2O_2	46.03	64-18-6
	Glyoxal	$C_2H_2O_2$	58.04	107-22-2
	Oxalic acid	$C_2H_2O_4$	90.03	144-62-7
TRIHEIA	1-(2-((2-hydroxyethyl)amino)ethyl)imidazolidin-2-one	$C_5H_{10}N_2O_2$	130.15	3699-54-5
TRIMEA	1-(2-hydroxyethyl)diethylenetriamine	$C_4H_{12}N_2O$	104.15	111-41-1

CHAPTER 1

INTRODUCTION

1.1 Motivation

The average temperature on the Earth has increased since the industrial revolution. This increase is mainly due to anthropogenic Greenhouse Gas (GHG) emissions[1]. These GHGs mainly consist of carbon dioxide (CO_2), water vapour (H_2O), methane (CH_4), nitrogen compounds (NOx) and sulphur compounds (SOx). The increased concentration of these gases increases the amount of absorbed solar radiation, resulting in an accelerating temperature increase[2]. This phenomenon is called *the greenhouse effect*. Increased average global temperature is of great concern as many species will become extinct, the sea level is rising, and even natural disasters occur more frequently[3].

In 1938, the British scientist G. Callendar linked the increasing combustion of fossil fuels and increased CO_2 concentration to the greenhouse effect[3]. CO_2 is believed to be the worst GHG as this gas has increased the most since pre-industrial levels. The most significant increase has mainly come from the combustion of fossil fuels, illustrated in Figure 1.1[4]. In the same figure, it can be seen that the *Intergovernmental Panel on Climate Change* or IPCC, reported a global increase in the annual GHG emission of 2.2% between 2000-2010.

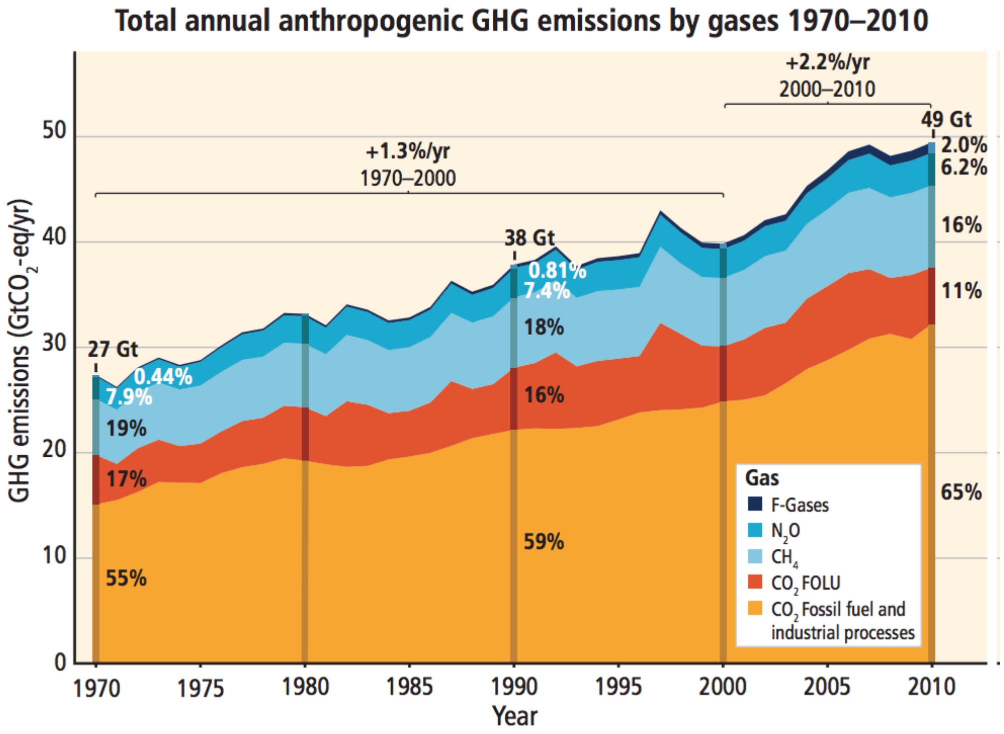

Figure 1.1: Global GHG emissions from 1970 to 2010[4].

CO_2 FOLU, illustrated as red in Figure 1.1, is the CO_2 emission from Forestry and Other Land Use. The most significant contributor to the massive GHG increase is the CO_2 from fossil fuels and other industrial processes, seen as orange. This contributor stood alone for 78% of the GHG increase from 1970 to 2010. A large portion of this comes from the energy sector. 25% of the total GHG emissions come from electricity and heat production[4]. That is over 12 Gt CO_2-equivalents annually from the energy sector if the total GHG emission is 49 Gt CO_2-equivalents like in 2010, shown in Figure 1.1.

In order to meet the Paris Agreement 1.5 °C goal from 2015, changes must be made. One can electrify the transport sector and use renewable energy sources to charge the batteries. Further, innovation can discover new technologies—for instance, fusion power and installation of other renewable sources for energy. Going to a clean green world takes time, and the need for energy is not likely to decline. The world's population is constantly growing. People are getting wealthier, which means more citizens will increase their energy consumption, food, and other factors that increase

GHG emission. Therefore, fossil fuels will most likely still be an essential source in the decades to come. The negative side is the extensive pollution of these sources of energy. Thermal power and particularly coal-fired power plants stood alone for 70% of China's energy installation in 2014[5]. The installation of carbon capture plants might be one solution to keep the global temperature down.

There are three main routes of CO_2 capture systems. Pre-combustion, oxy-fuel combustion and post-combustion. In pre-combustion, one removes the CO_2 produced in the water gas shift reaction when making H_2 from a syngas mixture of CO and H_2O. In the case of oxy-fuel combustion, coal burns with almost a pure excess of O_2. In oxy-fuel combustion, the CO_2 concentration in the flue gas is already almost concentrated enough for the requirements for transport and storage[6]. This report considers amine-based Post-combustion Carbon Capture (PCC), where CO_2 is captured from the flue gas exiting the combustion chamber. PCC is the CO_2 capture system that is easiest to retrofit in an existing power plant[7]. PPC can be utilised on flue gases from the energy sector or flue gases emitted by other industrial processes. A cement factory emits a significant amount of CO_2, where PCC can be applied as well[8].

The CO_2 content in the flue gases from coal-fired power plants is typically 12-14 vol%[9]. A CO_2 capture rate at 90% has often been used in the industry and research[10][11][12]. This means that one can reduce the global GHG emission by a great amount by utilising PCC technology on existing coal-fired power plants.

In amine-based PCC, the amine solvent counter-currently reacts with the CO_2 from the flue gas in an absorber column. The reverse reaction occurs in the desorber column, where CO_2 is released by additional heating. The solvent is recycled back and forth between these columns and constantly reused.

There are still some significant limitations with amine-based PCC. The process requires a great amount of thermal energy, often around 4 $\mathrm{GJ/t_{CO_2}}$ captured[13]. This means that the power plant reduces its net energy output by installing carbon capture technology. Besides the lower income due to the high energy demand, there is another major concern. This is solvent degradation. The solvent this work is based on is Monoethanolamine (MEA), which is one of the most studied solvents for PCC[14][15][16]. The published specific MEA loss by degradation in capture plants range between 0.3-3.6 kg MEA per ton CO_2 captured[10]. This solvent loss is expensive as new solvent must be purchased. Corrosion, foaming, and emission of volatile degradation compounds which are environmentally toxic are also of concern[17].

Degradation of the solvent leads to an accumulation of degradation products. Some of these products are organic acids, which provides a catalytic effect to corrosion. Corrosion is a problem as it damages the equipment, leading to a lower lifetime of the plant[18]. Furthermore, foaming leads to additional solvent loss, premature flooding and reduces the plant throughput. These consequences occur because of the physical properties of the degradation compounds[19].

A better understanding of solvent degradation is therefore essential for the PCC industry. This better understanding is required to evaluate the degree of degradation, the type of degradation compound and their impact on the operation and cost of the plants. This thesis is mainly based on solvent degradation; however, energy consumption in the process will also be considered.

1.2 Objective

The main objective of this work is to understand and predict solvent degradation in amine-based PCC. Two complete degradation models will be used to predict solvent degradation, where one is a complete simplified model, and the other is a complete advanced model. The models will be constructed and implemented in Python and validated. The models will be validated on a lab-scale experiment which was a campaign by SINTEF at a Solvent Degradation Rig (SDR) and a pilot plant at Niederaussem. Finally, the models will be used to compare degradation in a coal-based power plant and a Natural Gas (NG)-based power plant.

In the complete simplified model, a rate equation for the oxidative degradation will be developed in this work by fitting data using results from an oxidative degradation study by Vevelstad et al. (2014). The solubility of oxygen is in this model calculated based on equations from Weisenberger and Schumpe (1996), which is believed to be quite accurate. The thermal degradation in this model will be based on an in-house model at the Norwegian University of Science and Technology (NTNU).

The second complete degradation model is the advanced one. The oxidative degradation in this model is based on Pinto et al. (2014) and predicts, in addition to MEA consumption, the accumulation of degradation compounds. This model uses an oxygen solubility model developed by Rooney (1998), which is based on an unloaded solvent. Furthermore, another in-house model at NTNU is used to predict thermal degradation. This in-house model does also predict the accumulation of degradation compounds. The advanced model is constructed and implemented to evaluate which compounds are the most prominent in a PCC plant.

Both complete models will, in addition to oxidative and thermal degradation, include solvent degradation from impurities. These impurities consist of NOx and SOx, and the degradation rate is based on a study by Rao et al. (2002).

The models will be used at the SDR and the pilot plant at Niederaussem to find predicted consumption of MEA. The advanced model will also be validated with the prediction of degradation compounds.

Lastly, these models will be used to compare two industrial PCC plants. These cases are a degradation study from two hypothetical power plants. The first plant is a typical 400 MW coal-based power plant, and the second is a 400 MW NG-based power plant. The two cases will be simulated in the simulation tool *ProTreat*, where the temperature profiles in the absorber columns will be found. The specific MEA consumption [kg MEA/t_{CO_2}] will be investigated. The main goal here is to find potential differences in degradation based on the type of flue gas.

1.3 Outline of Thesis

The motivation and the objective of this thesis are given above. In Chapter 2 is where the theory about the PCC process, degradation, and energy demand is presented. Further, in Chapter 3 one can find the procedure of how the results are found. Assumptions that are used in the thesis are also introduced here. The results and discussion are to be found in Chapter 4. A conclusion of the thesis can be seen in Chapter 5 and further recommendations is found in Chapter 6. Additional results and information such as calculations and python code can be found in the Appendix, Chapter A.

CHAPTER 2

BACKGROUND

This Chapter includes theory on PCC, degradation, and the energy consumption of the reboiler. Section 2.1 is where the PCC process is described, and Section 2.2 gives the theory about solvent degradation. The proposed degradation reactions, which the models are based upon, will also be presented here. Lastly, Section 2.3 will cover the energy consumption in the reboiler.

2.1 Amine-based Post-combustion Carbon Capture

In Post-combustion Carbon Capture (PCC), flue gases are treated for CO_2 before leaving the stack. Flue gas from combustion is sent to the bottom of an absorber column. In this column, the flue gas rises to the top while counter-currently react with a chemical solvent in the column's packing. Most studies and this thesis are based on a 90% capture rate of CO_2[20], which means that only 10% of the original CO_2 emission is emitted. A capture rate of 90% is often used because a higher capture rate would significantly increase the energy consumption of the process.

The solvent is usually heated to some extent as the absorption process is an exothermic reaction. The solvent stream exits the absorber loaded with CO_2 and is pumped through a heat exchanger and then subsequently introduced into the top of the second column, known as the stripper or the desorber. Here, the solvent is heated additionally such that the reverse reactions are favoured. The loaded solvent releases CO_2 after being heated by the reboiler, which provides heat in the column. The CO_2 can be separated and transferred to the desired location. The now newly unloaded solvent is transferred back through the heat exchanger heating up the incoming stream to the desorber and back into the absorber. This process is illustrated in Figure 2.1.

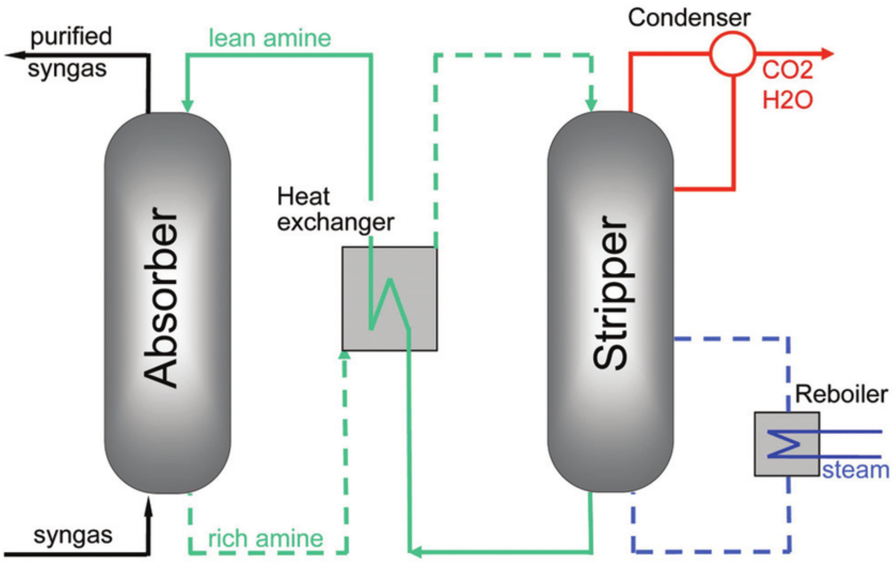

Figure 2.1: Simplified flow sheet of the PCC process[21].

A compatible solvent should have high selectivity towards CO_2, high maximum solvent loading, low lifetime cost, and low absorption enthalpy[22]. One of the most used solvents is MEA because of its high reactivity with CO_2[23]. The complete set of chemical reactions which occur in the PCC process is described by Equation 2.1 to 2.8[24].

$$CO_2 + H_2O \rightleftharpoons H_2CO_3 \tag{2.1}$$

$$CO_2 + OH^- \rightleftharpoons {HCO_3}^- \tag{2.2}$$

$$CO_3{}^{2-} + H^+ \rightleftharpoons HCO_3{}^- \tag{2.3}$$

$$HCO_3{}^- + H^+ \rightleftharpoons H_2CO_3 \tag{2.4}$$

$$RNH_2 + H^+ \rightleftharpoons RNH_3{}^+ \tag{2.5}$$

$$OH^- + H^+ \rightleftharpoons H_2O \tag{2.6}$$

$$CO_2 + RNH_2 \rightleftharpoons RNHCO_2H \tag{2.7}$$

$$RNH_2CO_2{}^- + H^+ \rightleftharpoons RNH_2CO_2H \tag{2.8}$$

Reaction 2.1 is the formation of carbonic acid, reaction 2.2 shows the formation of the bicarbonate and reaction 2.7 is the reaction with the amine to form carbamic acid. These are all slow measurable reactions. The rest of the equations illustrate instantaneous protonation equilibria reactions. Reaction 2.3 and 2.4 show the protonation of the carbonate. Reaction 2.5 is the protonation of the amine, reaction 2.6 is the protonation of the hydroxide, and reaction 2.8 shows the protonation of the carbamate[24]. For primary amines, such as MEA, the overall reaction between MEA and CO_2 is shown in Equation 2.9.

$$CO_2 + 2\,RNH_2 \rightleftharpoons RNHCO_2{}^- + RNH_3{}^+ \tag{2.9}$$

The equation above shows that one needs two amines (MEA) per CO_2 molecule. This stoichiometry is because the initially formed carbamic acid deprotonates and reacts with another MEA molecule[24]. The ratio between CO_2 moles and MEA moles is known as loading, often referred to as α, seen in Equation 2.10.

$$\alpha = \frac{n_{\mathrm{CO_2}}}{n_{MEA}} \tag{2.10}$$

The loading increases typically from 0.2 to 0.5 as the CO_2 from the flue gas is absorbed into the solvent. This means that a desorber column usually strips the solvent from the loading of 0.5 to 0.2. The reason for not stripping below this loading is the high energy demand, described in Section 2.3.

2.2 Degradation of MEA

Studies show that MEA degrades in the presence of O_2, NOx, SOx and at high temperatures[15][25]. The degradation has several adverse effects. Solvent degradation will lead to a lower solvent capacity, meaning that less CO_2 can be captured per time unit. Further, the new solvent must be purchased, which is a high cost. It is believed that the cost of this solvent make-up may stand for 22% of the operational expenses in an amine-based PCC plant[14]. In addition, degradation leads to corrosion, foaming and emissions of environmentally toxic degradation products[17].

Solvent degradation leads to corrosion because several known degradation products are acids, which increases the corrosion rate. Most of the CO_2 absorbers are built with carbon steel, mainly because of their low cost[18]. Corrosion of these steel equipment means a lower lifetime of the plant. Degradation products do also enhance the foaming tendency due to their physical properties. The foaming phenomena is of concern as it causes solvent loss, premature flooding and reduces the plant throughput[19].

In order to make PCC more economical and even more environmentally friendly, the energy consumption must be minimised, and solvent loss due to degradation should be as small as possible. Solvent loss may vary between 0.3 and 3.6 kg solvent per ton CO_2 captured[10]. For industrial-scale PCC plants, this will amount to a significant problem.

It has been reported that the highest loss of MEA is due to evaporation from the absorber. However, this problem can easily be reduced by having a water wash section installed. These emissions occur because MEA is relatively volatile. Svendsen et al. (2011) classified degradation compounds in three. The most volatile ones are ammonia and aldehydes. Non-volatile compounds are typically Heat Stable Salts (HSS) and organic acids, while low volatile compounds are in between, where MEA is classified. A water wash is a section in which the gas from the absorber is sent through before the gas exits the plant. This section contains a packed bed with continuous recycling of water, which has the goals to absorb the volatile compounds in the gas[26]. The bleed from the water wash is sent back to the absorber section. If the emissions still are significant with a water wash installed, additional water wash stages can be installed. Svendsen et al. (2011) proposed that by proper operation of water wash, the amine concentration in the flue gas exiting the water wash can come down to 0.01-0.05 ppm. A water wash can also reduce the emission of liquid entrainment, which are liquid droplets in the gas phase[16].

2.2.1 Oxidative Degradation

The second largest effect on solvent loss is believed to come from oxidative degradation[27]. Oxidative degradation occurs when MEA reacts with oxygen, which comes with the flue gas. Oxidative degradation reactions happen in the liquid phase, so O_2 must diffuse into the MEA for the reaction to occur[17]. The rate of oxidative degradation is increased with increasing temperature and oxygen content in the flue gas. For NG-based power plants, the rate of oxidative degradation might be even higher as more excess air is used, resulting in higher oxygen concentration[17]. However, the CO_2 concentration of these flue gases is usually lower than for coal-based power plants. The absorption of CO_2 is an exothermic reaction. This means that the temperature in the absorber might be higher in the absorber when the fuel is coal. The effect of the flue gas on degradation will be investigated in detail in the two industrial cases.

The amount of oxygen that is diffused into the solvent is referred to as oxygen solubility. The amount of oxygen in the solvent is rapidly increased when introducing richer oxygen content streams into the absorber. Further, the solubility decreases as the temperature and the loading of CO_2 increases[28]. This effect can also be seen in the seas. When the temperature in the oceans increases, it will lead to lower solubility of gases like CO_2, leading to constantly larger sieving of CO_2 from the seas.

Oxidative degradation mostly takes place in the absorber section. This is because the absorber section constantly has a supply of oxygen from the flue gas[29]. Therefore, it is assumed in this thesis that oxidative degradation only occurs in the absorber column and the absorber sump. However, it should be noted that the solvent can contain dissolved oxygen which has not reacted yet. The concentration may be small, but the temperature is higher, which increases the rate of oxidative degradation.

The oxidative degradation compounds in this report are based on the ones which were modelled by Pinto et al. (2014)[30] based on an oxidative degradation study conducted by Vevelstad et al. (2014). These include formaldehyde, formic acid, glyoxal, oxalic acid, HEF, HEI, BHEOX, HEGly and ammonia.

One major degradation compound which is not included in the model is HEPO. HEPO has in several articles been one of the most concentrated degradation compounds, and from a pilot campaign at Tiller, it accounted for over 50% of the degradation compounds[31]. The amount of HEPO was increased rapidly as the stripping temperature was raised to 140 °C, seen in an experiment by Leonard et al. (2014)[32]. The reason for not having HEPO included in the model and which consequences this have overall will be discussed in Section 4.2.2.

The chemistry of oxidative degradation is complex and not fully understood[33]. The advanced oxidative model used in this thesis is based on simplified reactions proposed by Pinto et al. (2014). The initial stage in oxidative degradation is believed to be a hydrogen abstraction mechanism, shown in Equation 2.11[30].

$$\mathrm{MEACOO^- + MEAH^+ + O_2 \longrightarrow 2CH_2O + CO_2 + 2NH_3} \tag{2.11}$$

Formaldehyde formed in this reaction is highly reactive and may react further with the solvent or other degradation compounds[31]. Equation 2.12 shows this as formaldehyde is an intermediate and is further oxidised to formic acid.

$$\mathrm{CH_2O + 0.5O_2 \longrightarrow CH_2O_2} \tag{2.12}$$

Furthermore, the formation of HEF is proposed to come from a reaction between protonated MEA and formate, shown in Equation 2.13.

$$\mathrm{MEAH^+ + CHO_2{}^- \longleftrightarrow HEF + H_2O} \tag{2.13}$$

Equation 2.14 shows the formation of $C_2H_2O_2$, the intermediate glyoxal. Additional ammonia is also formed. Glyoxal reacts with formaldehyde, MEA and ammonia further in Equation 2.15, forming HEI.

$$\mathrm{MEACOO^- + MEAH^+ + 2O_2 \longrightarrow 2C_2H_2O_2 + 2H_2O + 2NH_3 + CO_2} \tag{2.14}$$

$$\mathrm{MEA + CH_2O + C_2H_2O_2 + NH_3 \longleftrightarrow HEI + 3H_2O} \tag{2.15}$$

Glyoxal is also oxidised, forming oxalic acid, shown in Equation 2.16.

$$\mathrm{C_2H_2O_2 + O_2 \longrightarrow C_2H_2O_4} \tag{2.16}$$

Oxalic acid reacts in Equation 2.17 with MEA forming BHEOX.

$$\mathrm{2MEA + C_2H_2O_4 \longleftrightarrow BHEOX + 2H_2O} \tag{2.17}$$

Lastly, the formation of HEGly is shown in Equation 2.18.

$$MEACOO^- + MEAH^+ + O_2 \longrightarrow HEGly + NH_3 + H_2O + CO_2 \tag{2.18}$$

These are reactions used by Pinto et al. (2014), based on literature and observation in the oxidative degradation experiment by Vevelstad et al. (2014). There has also been observed a catalytic effect of dissolved metallic ions on oxidative degradation[34]. However, this effect has not been included in the models.

2.2.2 Thermal Degradation

Thermal degradation is reactions with MEA and CO_2 at elevated temperatures. This degradation path is mainly a problem in the desorber section, as this is where the temperature is the highest[34]. However, the temperature in the heat exchanger and the hot pipes are also relatively high, which means that thermal degradation of MEA can also occur here. In addition to temperature, the rate of thermal degradation is increased as the loading rises. This is because more CO_2 is present to react with MEA[35].

It should be noted that oxidative and thermal degradation are coupled, meaning that they both influence each other[30]. In this thesis, the models describing the oxidative and thermal degradation were developed independently, which means that this effect is not seen. The concentrations of the degradation compounds, which the advanced model predicts, might therefore differ from actual plants. This is a significant disadvantage in the model and will be discussed.

In order to describe the thermal degradation in the complete advanced model, an in-house degradation model is used. This in-house model uses equations similar to the ones by Davis (2009)[36]. The reactions that this model is based upon can be found in Equation 2.19 to 2.24. Thermal degradation in the complete simplified model is only described by the reaction in Equation 2.19, as this model only considers the consumption of MEA.

In the first reaction, seen in Equation 2.19, carbamate and protonated MEA is formed by a reaction between MEA and CO_2. It is assumed that the carbamate concentration is proportional to the CO_2 concentration, as long as there is enough MEA to form the carbamate.

$$\mathrm{2MEA} + \mathrm{CO_2} \longrightarrow \mathrm{MEAH^+} + \mathrm{MEACOO^-} \tag{2.19}$$

OZD is formed in Equation 2.20.

$$\mathrm{2MEAH^+} + \mathrm{MEACOO^-} \longrightarrow \mathrm{OZD} + \mathrm{MEA} \tag{2.20}$$

OZD is an intermediate and reacts with MEA to form HEEDA, as shown in Equation 2.21.

$$\mathrm{MEA} + \mathrm{OZD} \longrightarrow \mathrm{HEEDA} + \mathrm{CO_2} \tag{2.21}$$

HEEDA is believed to react with CO_2 and OZD, forming HEIA and TRIMEA, shown in Equation 2.22 and 2.23, respectively.

$$\mathrm{HEEDA} + \mathrm{CO_2} \longrightarrow \mathrm{HEIA} \tag{2.22}$$

$$\mathrm{HEEDA} + \mathrm{OZD} \longrightarrow \mathrm{TRIMEA} \tag{2.23}$$

Lastly, TRIMEA can react further with CO_2, forming TRIHEIA, shown in Equation 2.24.

$$\mathrm{TRIMEA} + \mathrm{CO_2} \longrightarrow \mathrm{TRIHEIA} \tag{2.24}$$

2.2.3 Degradation From Impurities

The last degradation path that the models are based on is degradation of MEA from impurities in the flue gas. Impurities such as SOx and NOx in the flue gas do also seem to cause degradation with MEA[32]. NOx usually contains 90-95% NO, with NO_2 being the remaining component. It is believed that NO_2 is the only component in the NOx which reacts with MEA[37]. Degradation with impurities is known to form nitrosamines. Even though the formation usually is not of great magnitude, these compounds are carcinogenic at low concentrations and are therefore essential factors in a degradation study[16][31].

2.3 Energy Considerations

The other major problem of amine-based PCC is the large energy consumption. Providing enough energy to reverse the absorption reactions is done in the reboiler section. Equation 2.25 can be used to find the total amount of energy, Q_{Reb}, which is divided into three parts[38].

$$Q_{Reb} = (\dot{n}_{\mathrm{CO}_2 \Delta H_{\mathrm{CO}_2}}) + (\overline{m}_{solv}\overline{C_p}(T_{in} - T_{out})) + (n_{vap,\mathrm{H}_2\mathrm{O}} H_{vap,\mathrm{H}_2\mathrm{O}}) \tag{2.25}$$

The first term in the equation above is the energy that is needed for the desorption process. $\dot{n}_{\mathrm{CO}_2}$ is the stripping molar flow rate, and ΔH_{CO_2} is the heat of CO_2 desorption. The second term represents the energy that is needed to provide the stripping temperature in the desorber section. $\overline{C_p}$ is the specific heat capacity of the solvent, and $(T_{in} - T_{out})$ is the temperature difference in the solvent for the inlet and outlet stream of the stripper, respectively. In the final term, $n_{vap,\mathrm{H}_2\mathrm{O}}$ is the molar flow rate of vaporised water and $H_{vap,\mathrm{H}_2\mathrm{O}}$ is the heat of water vapourisation. This term will increase when the driving forces are reduced. If the reboiler must strip to a low loading, the partial pressure of CO_2 is decreased and so are the driving forces for mass transfer in the system[39]. The partial pressure of water vapour must therefore be high, which increases the energy demand.

In order to limit energy consumption to a minimum, these terms should be considered when installing a carbon capture plant. The specific energy consumption is often measured to be GJ per ton CO_2 captured. The Liquid-to-Gas (L/G) ratio [kg solvent h^{-1} / kg flue gas h^{-1}] says how large the solvent flow rate is compared to the flue gas. An optimal L/G concerning energy will limit the energy consumption. If the solvent flow rate is too large, the second term in Equation 2.25 will increase more than necessary. But if the solvent flow rate is too low, the reboiler must strip to a lower lean loading, increasing the energy consumption exponentially, which is illustrated in Section 4.4.1.

CHAPTER 3

METHODOLOGY

In this Chapter, the procedure on how the results were obtained is shown. The lab-scale experiment and the pilot plant are introduced in Section 3.1. The solvent volumes being exposed to oxidative and thermal degradation will be assumed in Section 3.2. Section 3.3 and 3.4 are where the model equations are shown for the simplified and advanced model. Finally, Section 3.5 is where the methodology of the process simulations can be found. This section also includes a description of the industrial cases.

3.1 Experimental Studies

In this section, the lab and pilot plant with which the models are compared are introduced. The SDR campaign by SINTEF is described in Section 3.1.1. Then an introduction to the Niederaussem pilot plant can be found in Section 3.1.2.

3.1.1 SINTEF's Solvent Degradation Rig

Grimstvedt et al. (2020) investigated degradation in a Solvent Degradation Rig (SDR)[40]. This was a lab-scale degradation study that was run for eight weeks with 40 wt% MEA as solvent, where the concentration of MEA and degradation compounds were analysed every week through the campaign. In total, there were six different protocols in the campaign where process parameters were changed. In the first 3 weeks of the experiment, standard protocols were applied. In week 4-7, the concentration of NOx was increased, and in week 5-6 is when the stripping temperature was adjusted to 140 °C. Sump stripping was applied in week 5 and 8, and lastly, iron addition in week 7. Table 3.1 and 3.2 show the process conditions in the SDR[40].

Table 3.1: Process conditions in the SDR[40].

Weeks	Stripper Temperature [°C]	Desorber Pressure [bar]	Flue gas NOx content [ppmv]	Sump Stripping	Iron addition
Week 1-3	120	1.8	10	Off	No
Week 4	120	1.8	100	Off	No
Week 5	140	3.5	100	On	No
Week 6	140	3.5	100	Off	No
Week 7	120	1.8	100	Off	Yes
Week 8	120	1.8	10	On	No

Table 3.2: Additional process conditions in the SDR[40].

Lean loading	0.2
Rich loading	0.5
Flue gas flow rate [NL/min]	1
Flue gas temperature [°C]	40
Solvent volume [kg]	4.5
Initial MEA concentration [mol/L]	6.79
Flue gas composition	
O_2 [vol%]	12
CO_2 [vol%]	3
N_2 [vol%]	~75
NOx [ppm]	10-100

Table 3.2 shows the loading of the lean and rich solvent, flue gas flow rate, flue gas temperature, solvent volume, initial MEA concentration and the concentration of O_2, CO_2, N_2 and NOx in the flue gas.

The sump stripping was a method to remove oxygen and other trace gases dissolved in the solvent. The sump stripping was done by purging N_2 in the absorber sump, such that the partial pressure of oxygen and other trace gases was reduced, a benefit of Henry's Law. Overall, the sump stripping did no apparent effect in the experiment and is not considered in the models. The effect of iron addition was also not observed in the campaign. A simplified flow diagram of the SDR is illustrated in Figure 3.1.

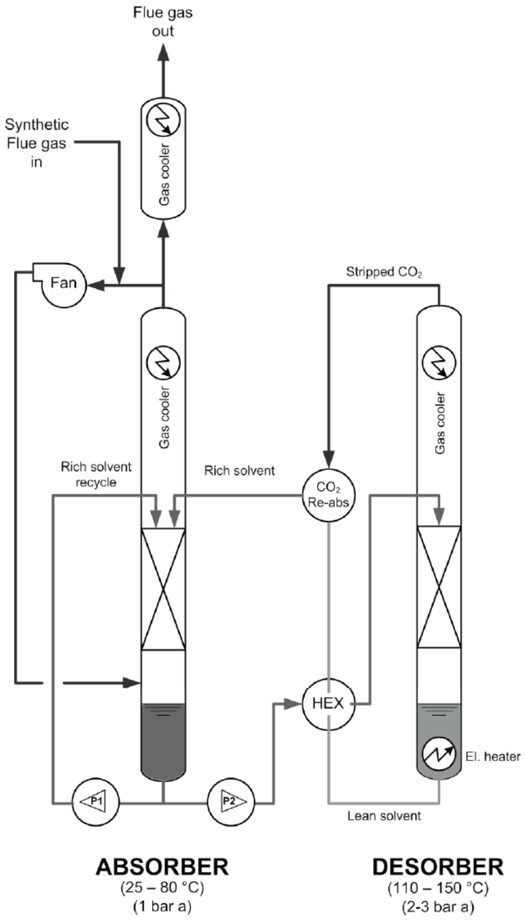

Figure 3.1: Flow diagram of the SDR[41].

Most of the absorption happened in the *Re-abs* (Re-absorber) by bubbling the flue gas through a filter covered by lean solvent. This Re-absorber was intercooled with tap water. Therefore, it was assumed that the average temperature in the Re-absorber was constant and equal to the temperature of the rich loading stream, being 40 °C. The rich stream was further sent to the absorber column. Both the rich solvent and the flue gas were recycled in the absorber column such that less synthetic flue gas was consumed and to get a realistic amount of solvent in the absorber.

The concentration of MEA and degradation compounds in the SDR were measured in mol/kg. The density of the lean solvent was around 1.09 g/mL[40]. Since the rich solvent density would be even higher as more CO_2 is present, an average density of 1.10 g/mL was assumed. This density was used to convert the concentrations into mol/L.

Grimstvedt et al. (2020) reported a relative MEA degradation of 3.6g/Lweek^{-1} where the main degradation compounds were HEPO, MEA urea, HEGly and HEEDA. It was further observed a clear effect of the degradation when the stripping temperature was increased[40]. Section 4.2 shows the results when the degradation models are applied to this degradation study.

3.1.2 Niederaussem Pilot Plant

Moser et al. (2020) investigated solvent degradation at a pilot-scale PCC plant at Niederaussem[10]. This campaign was an 18 month long test with a specific MEA consumption of 0.3 kg/t_{CO_2} in the first 4-5000 hours of operation. This MEA consumption is far less than what can be observed at other pilot plants, for unknown reasons[16]. The pilot plant had a 90% CO_2 capture rate with 30 wt% MEA as solvent[10]. Table 3.3 shows the process conditions at the pilot plant.

In this thesis, both complete models are predicting solvent degradation with process conditions at the Niederaussem pilot plant. It was chosen to model the first 4000 hours of operation, as this is where a linear degradation rate was observed at the plant. The degradation rate was increased to some extent after this period, which may have occurred due to iron catalysis. Since iron's effect on degradation is not included in the models, the linear degradation regime at Niederaussem was chosen to be modelled[10].

Table 3.3: Process conditions at the Niederaussem pilot plant[10].

Lean loading	0.2
Rich loading	0.5
Flue gas flow rate [m^3/h]	1150
Cold rich solvent temperature [°C]	40
Stripping temperature [°C]	120
Temperature in hot rich piping [°C]	110
Solvent volume [L]	3000
Initial MEA concentration [mol/L]	4.91
Flue gas composition	
O_2 [vol%]	5.0
CO_2 [vol%]	14.2
N_2 [vol%]	80.8
NOx [ppm]	130
SOx [ppm]	1

Moser et al. (2020) did not report the lean and rich loadings, so they were assumed to be 0.2 and 0.5, respectively. The solvent volume was found by a mail correspondence with Moser.

Since the cold rich solvent temperature was 40 °C, it was assumed that the average temperature in the absorber also was 40 °C. This is a relatively low temperature, as some temperature increase often is expected in the absorber due to the exothermic absorption reactions. With a CO_2 concentration above 14 vol%, the temperature might have increased significantly. However, no temperature profile was available, and that is why 40 °C was assumed. This might indicate that the models predict a reasonably low rate of oxidative degradation, as oxidative degradation is strongly dependent on the absorber temperature, which will be shown in Section 4.4.2.

By the first 4000 hours of operation at the Niederaussem pilot plant, 1000 tons of CO_2 was captured[10]. Section 4.3 shows how the two models compare with this pilot plant.

3.2 Solvent Volume Exposed to Degradation

In this section, assumptions are made to estimate how much solvent is exposed to oxidative and thermal degradation. Previous research has stated that the rate of oxidative degradation increases as the oxygen content and temperature increase. Likewise, thermal degradation is increasing as the temperature and loading are increasing. A campaign from the Technology Center Mongstad (TCM) published by Flø et al. (2017) estimated how much of the solvent was exposed in the different process components in the plant. According to this article, 44% of the solvent volume was at all time exposed to oxygen. This exposure to oxygen includes both the absorber and the absorber sump. An additional 35% of the solvent was exposed to temperatures above 100 °C. However, this part was divided into three, as the temperature and loading vary within each part[12].

The first volume, referred to as $V_{thermal1}$, is the solvent volume in the desorber packing, desorber sump, and reboiler. According to Flø et al. (2017), this volume is 9.5% of the total solvent volume. The temperature in this part is equal to the stripping temperature, and the loading is assumed to be equal to the lean loading[12].

The second volume, referred to as $V_{thermal2}$, is the volume of the hot rich piping. This part only contains 2.3% of the total volume, and the temperature is assumed to be 10 °C less than the stripping temperature. This was also seen at the hot rich piping in the Niederaussem pilot plant[10], as the temperature was 10 °C less than the stripping temperature. The loading is equal to the rich loading[12].

The last term, $V_{thermal3}$, represents the volume in the hot lean piping and the cross heat exchanger. By the estimation from Flø et al. (2017), this is 22.9% of the total volume. In this part, the temperature is assumed to be 10 °C less than the stripping temperature, the same as in the hot rich piping. It was further assumed that the CO_2 concentration is described by the lean loading[12].

When predicting MEA degradation in pilot plants and the industrial cases, these volumes are used. However, when modelling the SDR campaign by SINTEF, another assumption was made. This assumption is based on the configuration of the SDR, which was shown in Figure 3.1.

In this configuration, it was observed that there is a rich solvent recycling and a rich stream going to the desorber. In the SDR campaign, the rich solvent recycle had a volumetric flow of 10 L/h, while the stream going to the desorber had 6 L/h. This was taken into account when the degradation models were applied to this campaign. It was assumed that the stream passing through the whole rig followed the assumption from Flø et al. (2017), where 44% is in contact with oxygen. Furthermore, 60% of the recycle stream was assumed to be in contact with oxygen. Equation 3.1 shows the assumed total volume which is in contact with oxygen at the SDR.

$$V_{oxidative} = 0.44 \cdot (\frac{6}{16}) \cdot V + 0.60 \cdot (\frac{10}{16}) \cdot V = 0.54V \tag{3.1}$$

The equation shows that 44% of the volume of the stream going back and forth to the desorber is in contact with oxygen, while 60% of the solvent recycle stream is exposed to oxygen. In total, 54% of the solvent inventory is in contact with oxygen and therefore exposed to oxidative degradation.

The parts which were in contact with high temperatures, $V_{thermal1}$, $V_{thermal2}$ and $V_{thermal3}$, were calculated the same way, seen in Equation 3.2.

$$V_{thermal_i} = x_i \cdot (\frac{6}{16}) \cdot V \tag{3.2}$$

i is the number for each different part (1-3), and x_i is the fraction of volume at part i exposed to high temperature. These are presented above. The difference between the SDR, and pilot plants and the industrial cases is that the fraction of the volume is now split as 6/16 and 10/16, which represents the volumetric flows going through the whole rig and in the recycle.

3.3 Simplified Degradation Model

The first model referred to as the simplified model, only considers the consumption of MEA and does not include any degradation compounds. A rate equation for oxidative degradation was found in this work by fitting parameters from an oxidative degradation study by Vevelstad et al. (2014). This simplified model was developed to have a model for oxidative degradation, which takes loading into account when calculating the solubility of oxygen. The thermal degradation equation is an in-house model at NTNU.

3.3.1 Oxygen Solubility in Loaded MEA

The oxygen solubility depends on oxygen content in the gas, temperature, and solvent loading[29]. An oxygen solubility model by Weisenberger and Schumpe (1996) was therefore used. The model is suitable for electrolyte solutions between 2-5 kmol m^{-3} and is shown in Equation 3.3. The model uses experimental values from an experimental study by Buvik et al. (2021) and ion concentrations in CO_2-loaded 30 wt% MEA by Böttinger et al. (2008).

$$log\left(\frac{C_{G,0}}{C_G}\right) = \sum(h_i + -h_G)c_i \tag{3.3}$$

$C_{G,0}$ and C_G, inside the base 10 logarithm, are the gas solubility in pure water and electrolyte solutions, respectively. h_i is the ion-specific parameter, h_G is the gas-specific parameter, and C_i is the ion concentration. h_G depends on temperature, and its correlation with the temperature is given in Equation 3.4[29].

$$h_G = h_{G,0} + h_T(T - 298.15K) \tag{3.4}$$

$h_{G,0}$ is the gas-specific parameter, h_T is the temperature's effect of the gas-specific parameter, and T is the temperature. $h_{G,0}$ is 0 for oxygen ($h_{O_2,0}$) and h_T is -0.000334 $m^3kmol^{-1}K^{-1}$[42]. The ion-specific parameters for $MEAH^+$ and $MEACOO^-$ were determined to 0.0133 and 0.1284 m^3kmol^{-1} by Buvik et al. (2021). The ion-specific parameter for HCO_3 was determined to 0.0967 m^3kmol^{-1} by Weisenberger and Schumpe (1996). The ion concentration of $MEAH^+$, $MEACOO^-$ and HCO_3 were determined by NMR spectroscopic for a wide range of experiments by Böttinger et al. (2008)[43]. The ion concentrations used in this paper were taken from this experiment. These concentrations at the specific temperature and loading can be found in the python code in the Appendix, Section A.5.1[29].

The solubility of oxygen in pure water, $C_{O_2,0}$, was calculated by Equation 3.5 proposed by Xing et al. (2014)[44].

$$C_{O_2,0} = \frac{55.56 p_{O_2}}{exp(3.71814 + \frac{5596.17}{T} - \frac{1049668}{T^2} - p_{O_2})} \tag{3.5}$$

p_{O_2} is the partial pressure of oxygen [bar], and T is the temperature [K]. Buvik et al. (2020) found a low deviation in oxygen solubility between MEA solutions with 30 and 50 wt% MEA. Therefore, it was assumed that this model for predicting oxygen solubility is also valid for 40 wt% MEA solutions, like the MEA concentration at the SDR[29].

3.3.2 Oxidative Degradation Model

The rate equation for oxidative degradation in the simplified model is based on the experiments by Vevelstad et al. (2014). In this study, oxidative degradation was investigated in an open batch reactor containing 1 L 30 wt% MEA with a loading of 0.4[15]. Twelve different experiments were measured while varying the oxygen concentration and the temperature in the reactor. Three experiments out of these twelve were conducted with a gas phase oxygen concentration of 98 mol%. These three experiments were not included to obtain the rate of oxidative degradation. They were not included mainly because such high oxygen concentration is far from industrial levels. The temperature and oxygen concentration in the gas phase can be seen in Table 3.4 for the selected experiments.

Table 3.4: Temperature and oxygen concentration in the experiments by Vevelstad et al. (2014) which were used to fit the oxidative rate equation[15].

Temperature [°C]	Oxygen concentration [mol%]
55	6
55	21
55	49
65	6
65	21
65	49
75	6
75	21
75	49

The duration of the experiments varied between 20 and 42 days, and the MEA concentration was measured multiple times. For each of the selected nine experiments, five intervals were chosen to estimate a rate equation for oxidative degradation. Five intervals were chosen for each experiment to get a more robust rate equation.

The optimisation of the rate equation was done by the Nelder-Mead method and is seen in Section A.5.3 in the Appendix. The Nelder-Mead method optimised the pre-exponential factor to be 759 s^{-1} and the activation energy to be 52.1 kJ/mol, seen in Equation 3.6.

$$-r_{MEA,oxidative} = 759 \cdot e^{\frac{-52119}{R*T}} [\mathrm{O_2}]^{0.24} \tag{3.6}$$

R is the gas constant [8.314 J/Kmol], T is the temperature in the absorber [K] and $[O_2]$ is the concentration of oxygen [mol/L]. The rate of oxidative degradation, $-r_{MEA,oxidative}$ [mol/Ls^{-1}] depends on how much solvent is exposed to oxygen and is therefore multiplied with the solvent volume exposed to oxygen. This volume was described in Section 3.2.

3.3.3 Thermal Degradation Model

The rate equation for the thermal degradation in the simplified model comes from an in-house model[45]. This model with fitted parameters for the activation energy and pre-exponential factor in 30 wt% MEA, loading range between 0.1-0.45 and temperatures between 100-145 °C can be found in Equation 3.7.

$$-r_{MEA,thermal} = 3.34 \cdot 10^{-11} \cdot e^{\frac{-139000}{R}\left(\frac{1}{T}-\frac{1}{T_{ref}}\right)}[\mathrm{CO_2}][MEA] \tag{3.7}$$

$-r_{MEA,thermal}$ has units mol/m^{3}s^{-1}, and [CO$_2$] and $[MEA]$ have units mol/m^3. R is the gas constant [8.314 J/Kmol], T is the stripping temperature [K], and T_{ref} is a reference temperature of 400 K. In the model, this equation is divided by 1000, such that the unit of -r$_{MEA,thermal}$ is given in mol/Ls^{-1}, similar to the oxidative degradation equation.

As mentioned in Section 3.2, this rate equation must be multiplied with the volumes which have high temperatures. Therefore, the equation was split into three parts, Equation 3.8 to 3.10.

$$-r_{MEA,thermal,1} = 0.095 \cdot V \cdot 3.34 \cdot 10^{-11} \cdot e^{\frac{-139000}{R}\left(\frac{1}{T}-\frac{1}{T_{ref}}\right)}[\mathrm{CO_2}]_{lean}[MEA] \tag{3.8}$$

$$-r_{MEA,thermal,2} = 0.023 \cdot V \cdot 3.34 \cdot 10^{-11} \cdot e^{\frac{-139000}{R}\left(\frac{1}{T-10}-\frac{1}{T_{ref}}\right)}[\mathrm{CO_2}]_{rich}[MEA] \tag{3.9}$$

$$-r_{MEA,thermal,3} = 0.229 \cdot V \cdot 3.34 \cdot 10^{-11} \cdot e^{\frac{-139000}{R}\left(\frac{1}{T-10}-\frac{1}{T_{ref}}\right)}[\mathrm{CO_2}]_{lean}[MEA] \tag{3.10}$$

Equation 3.8 shows the thermal degradation occurring in the desorber, desorber sump and the reboiler, being 9.5% of the total volume. Equation 3.9 is the part that is in the hot rich piping, which is 2.3% of the total volume. The last one, seen in Equation 3.10, is the part in the hot lean piping, which is 22.9% of the total volume. 10 °C is subtracted from T in the latter two as the temperature here is lower than in the desorber. When the SDR is modelled, these equations are multiplied by 6/16, as mentioned in Section 3.2. It can also be seen that Equation 3.9 is the only one where rich loading is assumed, as the concentration of CO_2 is here equal to $\alpha_{rich}\cdot$[MEA].

3.3.4 Degradation from Impurities

The impurities of the flue gas, which consist of NO_2 and SO_2, both react with the amine. The contribution of these impurities in the flue gas is included in the model based on a study by Rao et al. (2002). Equation 3.11 shows this estimation[25].

$$[MEA]_{degradation} = 2f_{\mathrm{SO_2}} \cdot [\mathrm{SO_2}] + 2f_{\mathrm{NO_2}} \cdot [\mathrm{NO_2}] \tag{3.11}$$

Here, $[MEA]_{degradation}$ is the moles of MEA degraded per second, $f_{\mathrm{SO_2}}$ and $f_{\mathrm{NO_2}}$ are the reaction efficiencies of SO_2 and NO_2, and are 99.5% and 25%, respectively. [SO_2] and [NO_2] are the molar flows of the component in mol/s[25]. The reaction efficiencies are multiplied by 2 because two MEA molecules are reacting per SO_2 and NO_2. This equation for predicting MEA consumption from impurities are applied to both models.

3.4 Advanced Degradation Model

The complete advanced model in this thesis is based on Pinto et al. (2014) and an in-house model for thermal degradation, and lastly, the degradation from impurities by Rao et al. (2002). This complete advanced model can, in addition to MEA consumption, predict the accumulation of degradation compounds.

3.4.1 Oxidative Degradation Model

Pinto et al. (2014) fit the proposed oxidative degradation reactions based on the oxidative degradation study by Vevelstad et al. (2014). This model uses an oxygen solubility model developed by Rooney (1998). This oxygen solubility model does not take loading into account. The code which calculates this solubility is shown in Section A.5.2. These lines of code are taken from the previous work by Pinto et al. (2014).

In this oxidative model, no evaporation is assumed, which means that all of the formed degradation products remain in the liquid phase. Ammonia and formaldehyde are two volatile compounds that this may affect significantly. This means that the model's prediction of these compounds might be higher than what actually is in the solvent, as most can be assumed to exit with the gas. However, the model might fit describing the total amount of produced ammonia and formaldehyde.

Based on the proposed reactions describing oxidative degradation, shown in Section 2.2.1, reaction rate equations were fit by Pinto et al. (2014). The reaction rates, $R_{x,i}$ [mol/Lday^{-1}] with their respective reaction orders are shown in Equation 3.12 to 3.19. The value and units of the fitted pre-exponential factors, A$_i$ and activation energies, E$_{a,i}$ can be seen in Table A.1 in the Appendix, Section A.1[30]. The reaction order of the compounds are shown in the equations below.

$$R_{x_1} = A_1 exp\Big(\frac{-E_{A,1}}{RT}\Big)([MEACOO^-][MEAH^+])^{2.639}[\mathrm{O_2}]^{0.998} \tag{3.12}$$

$$R_{x_2} = A_2 exp\Big(\frac{-E_{A,2}}{RT}\Big)[Formaldehyde]^{0.936}[\mathrm{O_2}]^{0.107} \tag{3.13}$$

$$\begin{aligned} R_{x_3} = A_3 exp\Big(\frac{-E_{A,3}}{RT}\Big)[MEAH^+]^{0.657}[Formate]^{0.649} \\ -A_4 exp\Big(\frac{-E_{A,4}}{RT}\Big)[HEF]^{0.822} \end{aligned} \tag{3.14}$$

$$R_{x_4} = A_5 exp\Big(\frac{-E_{A,5}}{RT}\Big)([MEACOO^-][MEAH^+])^{0.598}[\mathrm{O_2}]^{0.785} \tag{3.15}$$

$$\begin{aligned} R_{x_5} = A_6 exp\Big(\frac{-E_{A,6}}{RT}\Big)[MEA]^{0.754}[\mathrm{CH_2O}]^{0.290}[\mathrm{NH_3}]^{0.961}[Glyoxal]^{1.169} \\ -A_7 exp\Big(\frac{-E_{A,7}}{RT}\Big)[HEI]^{0.643} \end{aligned} \tag{3.16}$$

$$R_{x_6} = A_8 exp\Big(\frac{-E_{A,8}}{RT}\Big)[Glyoxal]^{0.373}[\mathrm{O_2}]^{0.565} \tag{3.17}$$

$$\begin{aligned} R_{x_7} = A_9 exp\Big(\frac{-E_{A,9}}{RT}\Big)[MEAH^+]^{0.0.075}[Oxalate]^{0.230} \\ -A_{10} exp\Big(\frac{-E_{A,10}}{RT}\Big)[BHEOX]^{1.093} \end{aligned} \tag{3.18}$$

$$R_{x_8} = A_{11} exp\Big(\frac{-E_{A,11}}{RT}\Big)([MEACOO^-][MEAH^+])^{2.972}[\mathrm{O_2}]^{0.296} \tag{3.19}$$

It has been assumed that the formate concentration is equal to formic acid, and the concentration of oxalic acid is equal to oxalate. Theses assumption are based on instantaneous deprotonation of formic acid and oxalic acid. Also, the concentration of protonated MEA and carbamate is equal to the loading multiplied by the MEA concentration. These assumptions were made by Pinto et al. (2014).

3.4.2 Thermal Degradation Model

Since the development of an advanced thermal degradation model was beyond this project's scope, an in-house model was used. The rate equation describing the thermal degradation in the advanced model is seen in Equation 3.20. The reference reaction rate coefficient and activation energies were fit in previous work, where several experiments were included. These values can be found in Table A.2 in the Appendix, Section A.1.

$$k_{T,i} = k_{r,i} \cdot e^{\frac{-E_a}{R}\left(\frac{1}{T}-\frac{1}{T_{ref}}\right)} \tag{3.20}$$

$k_{T,i}$ is here the reaction rate coefficient for thermal degradation for reaction i, with units the same units as $k_{r,i}$. $k_{r,i}$ is the reference reaction rate coefficient with varying units. These units can be found in Table A.2. $E_{a,i}$ is the activation energy for reaction i [J/mol], T is the temperature [K], R is the gas constant [8.314 J/Kmol], and T_{ref} is the reference temperature at 400 K.

The in-house model for thermal degradation is based on the chemical reactions, given in Equation 2.21-2.24, Section 2.2. The rate equations for these reactions can be seen below, from Equation 3.21 to 3.24.

$$R_{T_1} = k_{T,1}[\text{MEACOO}^-] \tag{3.21}$$

$$R_{T_2} = k_{T,2}[HEEDA][\text{CO}_2] \tag{3.22}$$

$$R_{T_3} = k_{T,3}[HEEDA][\text{MEACOO}^-] \tag{3.23}$$

$$R_{T_4} = k_{T,4}[TRIMEA][\text{CO}_2] \tag{3.24}$$

The values of $k_{T,i}$ were calculated by Equation 3.20, and multiplied with the compound concentrations, seen from Equation 3.21 to 3.24. These equations are based on concentration units of [mol/m^3]. The units are converted from mol/L to mol/m^3 by multiplying the concentrations with 1000 L/m^3. The rate of reactions are finally divided by 1000 such that the equations return mol/Ls^{-1}. This can be seen in the advanced model in the Python code in the Appendix, Section A.5.5.

3.5 Modelling Industrial Cases

In the final part of this thesis, the two degradation models are applied to two different fossil power plants. These two fossil powered plants are assumed to have a PCC installed using 30 wt% MEA as solvent. This part aimed to find the main differences in degradation by either having coal or NG as fuel in a power plant. In this section, the methodology in how the results were obtained are described. First, a typical flue gas flow rate and composition from industrial-sized coal and NG-based power plants were found. Then simulations in ProTreat were done to find the optimal L/G ratio concerning the energy need in the reboiler. By studying the temperature profiles of the absorber with the optimal L/G, an average temperature was found. The dimensions for the absorber and desorber column were found by assumptions and by literature.

The case for the hypothetical coal-based power plant has its flue gas flow and composition taken from a typical 400 MW plant, described by Singh et al. (2003)[11]. The NG flue gas flow rate is also taken from a typical 400 MW power plant, which was found in an article by Sipöcz et al. (2011)[46]. Amann and Bouallou. (2009) made a simulation comparison between NG and coal-based power plants, which is from where the flue gas composition of the NG is taken[47]. The flow rates and compositions of the flue gases can be seen in Table A.3 in Section A.4 in the Appendix. The absorber and desorber pressures were chosen to be 1.0 and 2.0 bar, respectively. These are typical pressures for industrial sized plants[48][11].

3.5.1 Simulation

For the simulation part in this thesis, heights of the absorber and desorber columns were needed. The height of the absorber column was set to be 20.0 meters, equal to the height of the Tiller pilot plant. Likewise, the height of the desorber column was set to 13.7 meters, similar to the Tiller pilot plant. The heights of these columns at Tiller were based on industrial sized column[49]. However, the diameters in the Tiller pilot plant columns were not scaled for an industrial plant. Therefore, the diameters were calculated based on the flow rate of the gas and the gas velocity, given by Equation 3.25[50].

$$\dot{V} = Av \tag{3.25}$$

In Equation 3.25, the cross-section area A [m^2] was calculated by dividing the flow rate of the flue gas, $\dot{V}$ [m^3/s], by the gas velocity, v [m/s]. Park and Øi. (2017) estimated the capital cost of absorber columns concerning the gas velocity. In that work, it was found that the optimal gas velocity for a typical Mellapak 250Y packing is 2.0 m/s for flue gases emitted by the combustion of natural gas[50]. The gas velocity of 2.0 m/s was also used on the flue gas from the coal study. In the Tiller pilot plant, the desorber has a diameter equal to 80% of the absorber diameter. The diameter of the desorber was therefore assumed to be 80% of the absorber in this thesis. The calculated diameter for both cases can be found in Table A.3 in Section A.4 in the Appendix. A screenshot of the simulation in ProTreat can be seen in Figure 3.2.

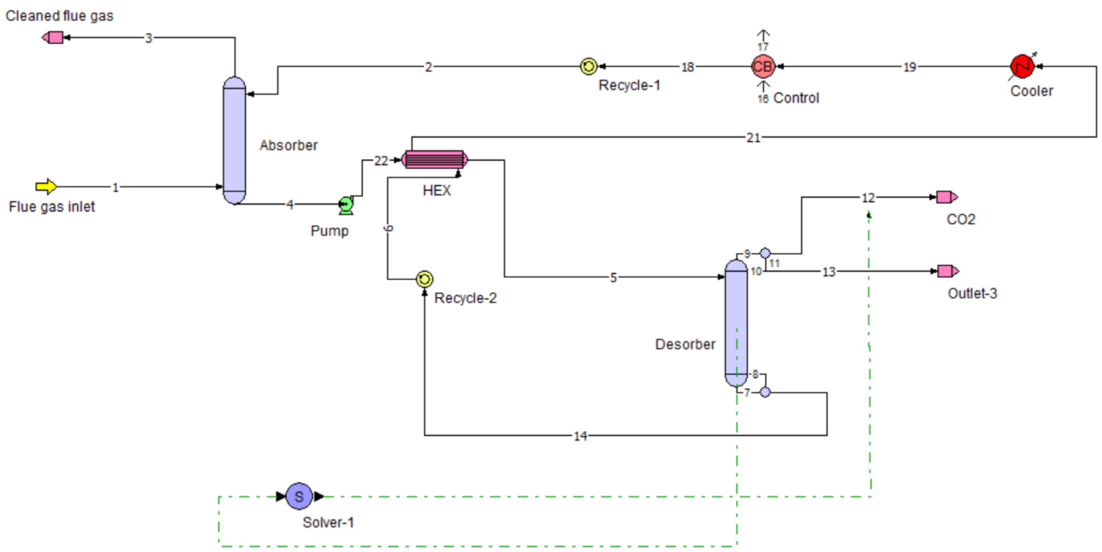

Figure 3.2: Screenshot from the industrial case simulation in ProTreat.

The flue gas comes in with stream *1* at 40 °C at 1.0 bar to the absorber. Here, the CO_2 counter-currently reacts with a 30 wt% MEA solution, stream *2*, which enters the absorber at the top. The rich solvent is pumped through the heat exchanger, *HEX* and enters the desorber column with stream *5*. HEX is a pinch-exchanger with a minimal approach temperature of 10 °C. A pinch temperature of 10 °C has been used in previous research and was therefore also used here[51]. Further in the desorber, the rich solvent is stripped for CO_2, before the rich CO_2-stream is cooled with a condenser. This condenser was set to 20 °C, such that a 98.7 mol% pure CO_2 stream could exit with stream *12*. Stream *13* is water that was separated from the rich CO_2-stream in the condenser, and stream *10* is the water reflux back to the desorber. *Solver-1* is the adjustment block, which adjusted the reboiler duty such that 90% of the CO_2 from stream *1* was stripped. The lean solvent in stream *14* passes the heat exchanger heating the stream from the absorber and is further cooled down to 40 °C in the *Cooler*. *Control* is the block that provides additional make-up values of water and MEA. The two recycle blocks were included to set initial values such that the simulation converged.

22 simulations were run for the coal flue gas, where the L/G ratio varied between 2.0 and 7.0. The run with the lowest reboiler duty was chosen to have the optimal L/G concerning energy consumption. A temperature profile was found in ProTreat

and used to calculate an average temperature in the absorber column. Additional 17 simulations were run for the NG flue gas. These simulations had an L/G value ranging between 0.75 and 4.0, and the optimal L/G concerning energy was found. The temperature profile for this run was also found, such that an average temperature was calculated. The average temperatures in the absorber were found by assuming that the liquid flow was constant through the packing.

For the degradation study, concentrations of NOx and SOx were found based on literature for the two cases. The concentration of these impurities for the coal flue gas was assumed to be equal to the concentration found in Niederaussem, 150 mg/Nm^3 ($\sim$130 ppm) NOx and 1 mg/Nm^3 ($\sim$1 ppm) SOx. Häsänen et al. (1986) did an emission comparison study on NOx in coal and NG power plants. It was found that the NOx emission was 300 mg/MJ for coal and 100 mg/MJ for NG. The NOx concentration in the flue gas from NG was set to 43 ppm, or 33% of the NOx assumed in the coal flue gas. It was further assumed that no SOx is found in the flue gas from the NG power plant.

The total solvent inventory in the two cases are based on the volume which was found at Niederaussem. Since the Niederaussem pilot plant captured 1000 tons CO_2 in 4000 hours, it had an hourly CO_2-absorption rate of 250 kg/h. The plant had a total volume of 3000 L, which means that 12 L solvent was needed per kg CO_2 absorbed per hour. Based on the hourly CO_2 capture rate from the simulations at a 90% CO_2 capture rate, the total solvent volumes were calculated. The results from these calculations can be found in Table A.6, in Section A.4.

CHAPTER 4

RESULTS AND DISCUSSION

In this Chapter, both degradation models are evaluated and used. Section 4.1 is where the parameter fitting of the oxidative degradation equation for the simplified model is discussed. Secondly, Section 4.2 is where the models are compared with SINTEF's SDR campaign. In addition to MEA consumption, the advanced model is compared by modelling the accumulation of the degradation compounds. Then, the models are used to predict degradation at the Niederaussem pilot plant in Section 4.3. Finally, the simulation results from the industrial cases are shown in Section 4.4. This study is done to find potential differences regarding degradation with different types of fossil fuel. The flue gas from the NG-based power plant has more oxygen in the flue gas. However, the coal flue gas has more CO_2 indicating more heat from the absorption in the absorber column.

4.1 Fitting the Oxidative Degradation Equation

The parameter fitting was done to get a rigid rate of oxidative degradation in the simplified model. The constants in Equation 3.6 was fitted. It was chosen to use 45 intervals to fit this equation to have a sufficient amount of data points. Figure 4.1 shows how the 45 chosen measurements by Vevelstad et al. (2014) compare with the optimised oxidative degradation equation. This comparison aimed to see if any trends could indicate over or under-prediction of the obtained rate equation. The ratio between the predicted MEA consumption by the model divided by the observed change in the MEA concentration is plotted against four different parameters to see if there are any trends. The red horizontal line indicates where the model yields the same degradation as the experiment. This means that the blue points above the red line are where the model is over-predicting the amount of MEA degraded. The points that are below the red line indicate an under-prediction of the model compared to the experiment.

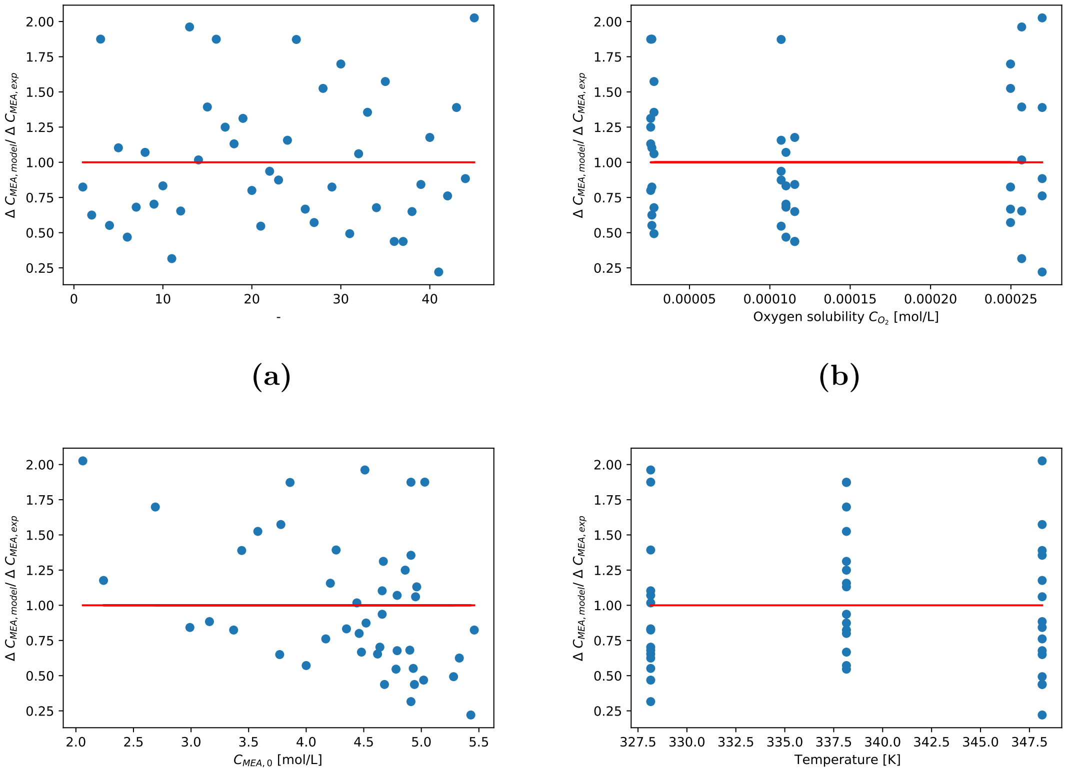

(a) **(b)**

(c) **(d)**

Figure 4.1: Ratio between the change in MEA concentration between the model and the experiment by Vevelstad et al. (2014) plotted against each run (4.1a), oxygen solubility (4.1b), initial MEA concentration (4.1c) and temperature (4.1d)[15].

In Figure 4.1a, the change in MEA concentration predicted by the model divided by the MEA change in the experiment is plotted against the 45 intervals. The points are scattered, and it is hard to distinguish if there are any reasons for the widespread because of the parameters like oxygen solubility, initial MEA concentration and temperature change. Therefore, three additional plots were made such that any possible trends can be discovered.

Figure 4.1b shows the difference between the model and the experiment with varying oxygen solubility. There are three bulks of points in this plot, where the bulk to the far left contains the measurements with 6 mol% O_2, the middle one is with 21 mol% O_2, and the last one to the far right is when the oxygen concentration was 49 mol%. The temperature dependency of oxygen solubility is the reason for the small spread on the x-axis in every main bulk, as the temperature ranged between 55 and 75 °C. An almost equal amount of points at both sides of the red line can be seen for every bulk, except the middle one with 21 mol% O_2 where most are below. However, no clear trend can be found.

Further, in Figure 4.1c, the change in MEA concentration ratio is plotted against the initial MEA concentration in the interval. Neither in this figure can a trend be found. It is known from the literature that oxidative degradation also depends on the MEA concentration in addition to O_2[52]. Therefore, in this figure it was tried to see any difference between high and low MEA concentrations. However, it looks like the rate equation fits evenly well for all concentrations.

The last comparison, Figure 4.1d, shows the accuracy of the model compared with temperature. The points are above and below the red line for all three temperatures of the experiment. Neither here can a trend be found.

Based on the illustrations in Figure 4.1, it can be concluded that the obtained rate equation describing the oxidative degradation in the simplified model fits averagely good. No trend indicates that the rate equation is a bad fit. However, ideally, should a rate equation have been fit with more data.

4.2 Modelling the Solvent Degradation Rig

This is the section where the lab-scale experiment is modelled. The MEA consumption is modelled in Section 4.2.1 and the degradation products are modelled in Section 4.2.2.

4.2.1 MEA Consumption

In this section, both models are used to predict the MEA consumption in the SDR. Figure 4.2 shows how the simplified and advanced model fit the measured MEA concentrations at the SDR.

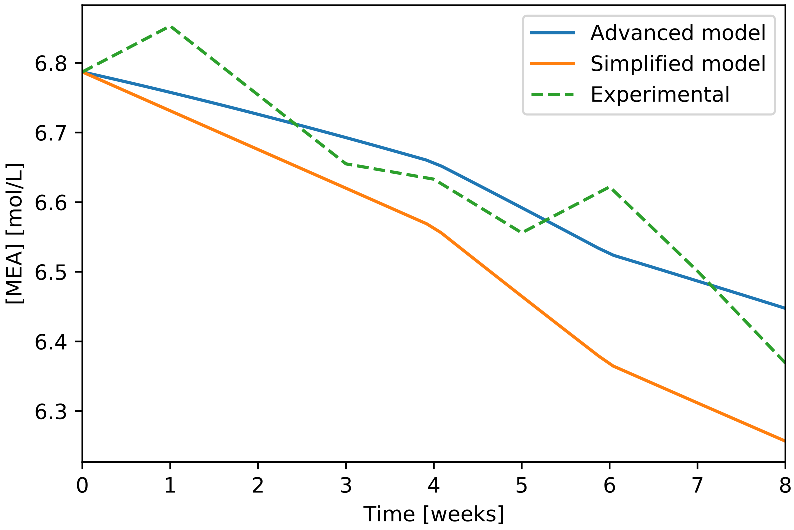

Figure 4.2: Models prediction of MEA consumption at the SDR[40].

One can see in Figure 4.2 that the advanced model is plotted as a blue line, the simplified model is the orange line, and experimental values from the SDR is illustrated with the dashed green one. This green line is based on 9 measurements, one initially and then one for each week. It can be seen that the simplified model predicts more degradation than the advanced model and the experiment. The advanced model is more accurate and is slightly under-predicted at week 8. The simplified model predicts an MEA concentration of 6.3 mol/L, and the advanced predicts 6.4 mol/L after

8 weeks of operation. The final concentration in the experiment was 5.79 mol/kg, or 6.37 mol/L based on a density of 1.1 g/ml[40].

The reason for the concentration increase seen in week 1 in the experiment is unknown. The concentration increase from week 5 to 6, however, is the outcome of a leakage in the rig. 0.5 kg virgin 40 wt% MEA was refilled, which is the reason for the concentration hop from week 5 to 6. Despite these two concentration hops in the experiment, it seems like the concentration decreased quite linearly. However, it can be observed that the rate of degradation was increased from week 4-5 at the SDR. This is when the stripping temperature was increased to 140 °C, and can also easily be observed in the models.

Both oxidative degradation models were fitted with the same data, but they are still different, which might be because of the different solubility models they are based upon. The advanced model has a solubility model by Rooney (1998) which, calculates the solubility of oxygen in unloaded MEA[53]. Meanwhile, the simplified model uses the oxygen solubility model which also includes the CO_2 loading.

4.2.2 Degradation Products

In this part, the advanced degradation model is used to compare accumulated degradation products in the SDR. Figure 4.3 shows the model's prediction of NH_3, HEF, HEI and HEGly.

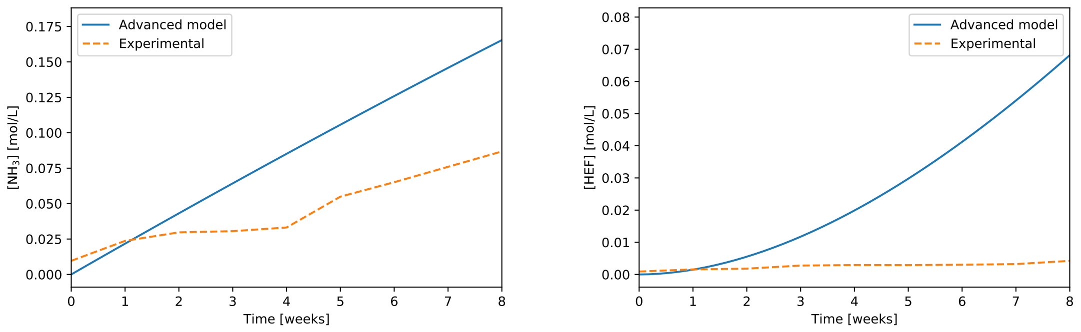

(a) NH_3 **(b) HEF**

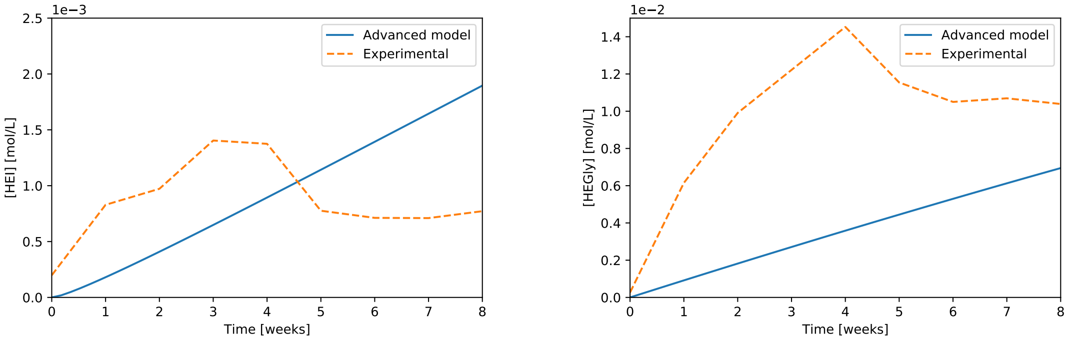

(c) HEI **(d) HEGly**

Figure 4.3: The advanced model's prediction on NH_3 (4.3a), HEF (4.3b), HEI (4.3c), and HEGly (4.3d) illustrated by the blue line compared with the measured experimental concentration, illustrated with the orange dashed lines[40].

Figure 4.3a shows the model's prediction of ammonia. The concentration in the first week fits quite well, but the model is then constantly over-predicting the amount of ammonia. One crucial difference in the model and the SDR when comparing ammonia is that ammonia is volatile. Therefore, some of the dissolved ammonia in the SDR is continuously vaporised. The model does not include the volatility of ammonia and predicts the total amount of formed ammonia in the liquid phase. Because of this vaporisation, the total amount of formed ammonia could be more significant in the SDR than what the figure shows. This means that the model might be more precise in determining the accumulation of ammonia, but since some are constantly vaporised, the concentration is off. SINTEF measured the ammonia emission of a similar SDR campaign in 2012. Typically measured emission values were in the range 164-267 mg/Nm^3 in the flue gas. However, these measurements were strictly qualitatively correct, so the accuracy of these emission results might range from a factor of ten[40]. The emissions of ammonia at other pilot plants have varied between 200-300 mg/m^3[10]. Overall, the model might fit quite well, but the disadvantage of not including evaporation in the model results in uncertainty in this prediction.

Figure 4.3b shows that the model's prediction of HEF does not fit with the measured concentration. The model predicts an exponential increase of HEF, while the experimental measurements were slightly positively linear. In the model equilibrium reaction, shown in Equation 3.14, it can be seen that HEF is produced if the concentration of formate is large, by Le Chatelier's principle. This will be discussed more in detail later when concentration profiles of formaldehyde and formic acid are shown.

The next component to which the model is compared is HEI, seen in Figure 4.3c. It seems like the model is under-predicting during the first 4 weeks and then over-predicting during the last weeks. It looks like Equation 2.15 was shifted left after week 4 in the SDR campaign, as the concentration of HEI was reduced while the concentration of ammonia increased. So the difference between the experiment and the model might come from the stripping conditions. This comes from the limitation previously described, the fact that the oxidative model is based on pure absorber conditions. However, it seems like the model fits quite well during the first 4 weeks when the stripping temperature was 120 °C. Since HEI is a product of ammonia, formaldehyde and glyoxal, the limiting factor may be glyoxal as ammonia and formaldehyde have relatively high concentrations.

Figure 4.3d shows the formation of HEGly. Here, it can be seen a rapid increase of accumulation initially at the SDR followed by a decrease at week 4 when the stripping temperature was increased. This decrease is most likely because HEGly is a known intermediate forming HEPO. It was observed that the HEPO concentration increased significantly from week 4 at the SDR[40]. Since HEPO is not included in the model and instead predicts HEGly as an end-product, it may be expected that the predicted concentration of HEGly is most precise in the first weeks. Then, after some time, the model would over-predict the concentration of HEGly. HEPO was not included in the model by Pinto et al. (2014) because the reaction rates were based on a purely oxidative study. In this study, used to fit the oxidative model, a minimal concentration of HEPO was observed and is most likely because of the absence of high temperature stripping conditions.

Figure 4.4 shows the formation of formic acid, formaldehyde, HEEDA, and HEIA.

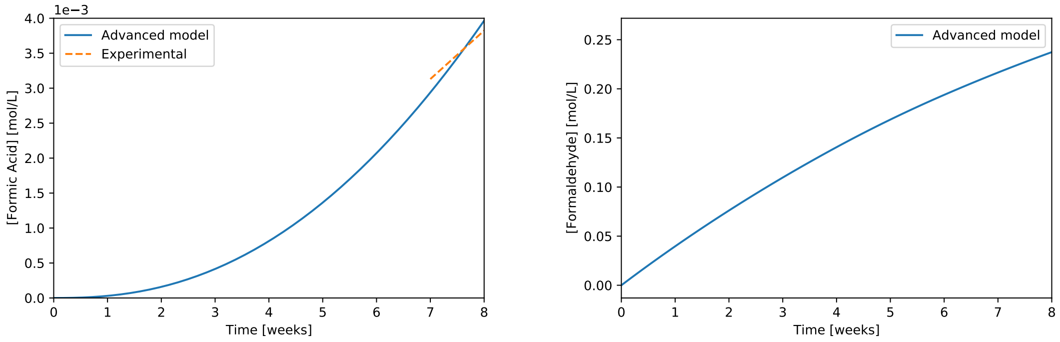

(a) Formic acid

(b) Formaldehyde

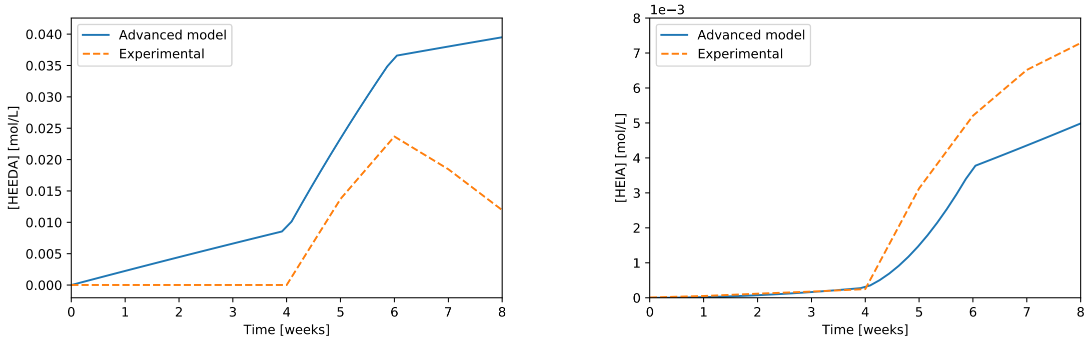

(c) HEEDA

(d) HEIA

Figure 4.4: The advanced model's prediction on formic acid (4.4a), formaldehyde (4.4b), HEEDA (4.4c) and HEIA (4.4d) illustrated by the blue line compared with the measured experimental concentration, illustrated with the orange dashed lines[40].

In Figure 4.4a, the formic acid is modelled. Here, the orange dashed lines that show the measured concentration of formic acid in the SDR start at week 7. The reason for this is because the measured concentrations in the previous weeks were below the detectable limit. However, in week 7 and 8, the concentration was detected and very close to what the model predicted. Formic acid was proposed as a product of formaldehyde, which was shown in Equation 2.12. It can be seen that the behaviour in the formation of HEF in Figure 4.3b is similar to the formation of formic acid. This is most likely because formate, which was assumed to have the same concentration as formic acid, reacts with protonated MEA to form HEF, seen in Equation 2.13. Since the concentration of formic acid seems well modelled, the assumption of $C_{formate} = C_{formic\ acid}$ might have been the reason for the large over-prediction of HEF formation in the model. So, the deprotonation of formic acid to formate might be lower than was assumed in the model.

Formaldehyde is one of the most significant degradation compounds in this model, seen in Figure 4.4b. There are no dashed orange lines in this figure because formaldehyde was not analysed for at the SDR. According to Svendsen et al. (2011), formaldehyde is amongst the most volatile compounds seen from degradation of MEA[54]. This might have been why SINTEF did not analyse for formaldehyde in the solvent, as most of the formaldehyde was vaporised. Therefore, the concentration of formaldehyde predicted by the model is not reliable, as a great portion can be assumed to be vaporised. This means that the model's prediction of formaldehyde, in addition to ammonia, most likely over-predicts.

Figure 4.4c shows the concentration of the thermal degradation compound HEEDA. The behaviour of the model and the measured concentration seems to be equal, with some exceptions. A relatively large increase can be observed for both cases as the temperature was increased to 140 °C from week 4. After week 6, the model predicts a slight linear increase while the concentration at the SDR slowly decreased. HEEDA was proposed to be an intermediate forming HEIA and TRIMEA, shown in Equation 2.22 and 2.23, respectively. TRIMEA was not analysed for in the SDR, but HEIA seems to have the same increase as the model seen in Figure 4.4d. There was a significant increase in HEPO in the final weeks in the SDR, and a proposed reaction with HEEDA forming HEPO can explain the observed decrease from week 6[55]. Léonard et al. (2014) found a similar behaviour of HEEDA and HEIA. In his experiment, the concentration of HEEDA was dominating with a stripping temperature of 120 °C. When the stripping temperature was 140 °C, however, it looked like HEEDA reached a plateau. And from this point, the formation of HEIA was dominating[56]. Figure A.2 in the Appendix shows that HEIA would also be the main thermal degradation product after a longer period.

The formation of HEIA seems, according to Figure 4.4d, quite well for the model. As HEIA was suggested as an end product formed by HEEDA, HEIA would increase with increasing concentration of HEEDA. A slight under-prediction can however be observed in the model. It looks like HEEDA is degrading to HEIA faster in the SDR than the model.

Figure 4.5 shows the model's prediction for the rest of the compounds included in the model.

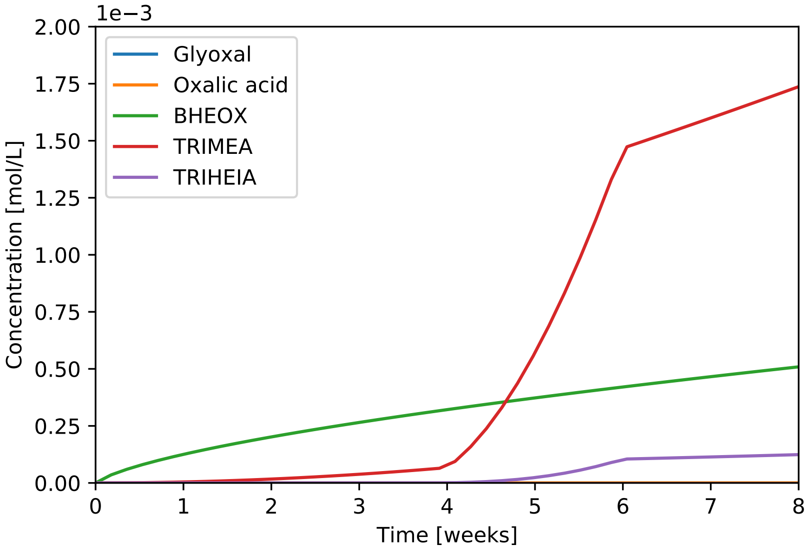

Figure 4.5: Predicted concentration of the minor compounds which were not analysed for at the SDR.

In this figure, the concentration increase of TRIMEA is the largest, especially from week 4-6 with high stripping temperature. TRIMEA was proposed as an intermediate transforming to TRIHEIA, which also had a concentration increase from week 4. BHEOX is formed from oxalic acid by Equation 2.17. It looks like all formed oxalic acid is transformed to BHEOX, and all formed glyoxal is oxidised to oxalic acid since the concentration of both oxalic acid and glyoxal are more or less zero through the period. This shows that glyoxal is the limiting factor producing HEI, which was mentioned earlier. The rest of the glyoxal reacts with oxygen forming oxalic acid (Reaction 2.16) and further reacts with two MEA molecules producing BHEOX (Reaction 2.17). BHEOX was measured in the SDR, but this was only a condensate measurement after the absorber and not in the liquid phase. However, the concentration of BHEOX in the condensate was small, and it looks like it was linearly growing, which fits this model[40].

Overall, the advanced model seems to fit quite well with the MEA consumption observed at the SDR. The model also has similar behaviour for most of the analysed degradation compounds. Although, some limitations have been mentioned. The oxidative part of the model was developed from a purely oxidative study, which means that compounds like HEPO were not included. This means that HEGly might be over-predicted, especially after a more extended period. At week 8 in the SDR campaign, SINTEF observed that HEPO accounted for approximately 60% of the oxidative degradation compounds[40], while in the model, formaldehyde is the most dominating compound. The concentrations of formaldehyde and ammonia are believed to be lower than the model predicts as they are volatile and may evaporate[40].

It might look like the assumptions of the volume fractions, which were in contact with oxidative and thermal degradation, fit quite well in this campaign. However, in the future, the solvent volumes exposed to oxidative and thermal degradation should be measured from the SDR.

Figure A.1 and A.2 in the Appendix, Section A.2 shows the model's prediction of the SDR over 80 weeks for oxidative and thermal degradation, respectively. After week 8, standard protocols were applied to find potential steady state values of the compounds. In Figure A.1 it can be seen that the formaldehyde concentration decreases after some time while HEF and formic acid increase. This figure shows that HEF and formic acid are the compounds with the highest formation rate after 80 weeks. HEF is, however, decreasing some, which indicates that formic acid (which is assumed to be equal to formate) will increase even more.

For the thermal degradation compounds, seen in Figure A.2, it is observed that

HEIA will be the most significant product after some time, which also was seen in the experiment by Léonard et al. (2014). This fits with the theory that HEEDA is an intermediate and transforms to HEIA. TRIMEA and TRIHEIA are also growing while it looks like HEEDA reaches a plateau.

4.3 Modelling the Niederaussem Pilot Plant

In this section, the two models are compared with the Niederaussem pilot plant. The Niederaussem pilot plant was described in Section 3.1.2. Figure 4.6 shows the models prediction of the Niederaussem pilot plant, based on the data from Moser et al. (2020) and the assumptions from Section 3.1.2 and 3.2.

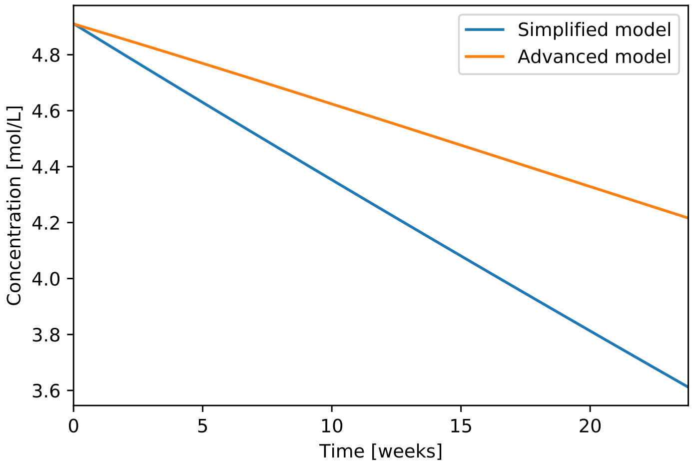

Figure 4.6: The models prediction of the MEA consumption at the Niederaussem pilot plant over 24 weeks (4000 h).

Figure 4.6 shows a significant difference between the models when comparing the MEA consumptions at Niederaussem. The blue line, the simplified model, predicts an MEA concentration of 3.6 mol/L, while the advanced model, the orange line, predicts an MEA concentration of 4.2 mol/L after 4000 hours. The specific MEA consumption for both models can be found in Table 4.1.

Table 4.1: Specific MEA consumption for the two models predicted on the pilot plant at Niederaussem.

	Simplified model	Advanced model
Δ C_{MEA} [mol/L]	1.33	0.69
Solvent volume [L]	3000	3000
CO_2 captured [ton]	1000	1000
MEA degraded [kg]	243	126
MEA consumption [kg MEA/t_{CO_2}]	0.243	0.126

The specific MEA consumption at Niederaussem was below 0.3 kg MEA/t_{CO_2} during the first 4000 hours[10]. It can be seen that the simplified model fits quite well with a specific MEA consumption of 0.24 kg MEA/t_{CO_2}. The advanced model predicts 0.13 kg MEA/t_{CO_2}, approximately half the degradation observed at Niederaussem. A reason for the large difference between the models may be that the advanced model depends more on temperature than the simplified model, in addition to the different oxygen solubility models. The temperature dependency will be further discussed in Section 4.4.

Some of the under-prediction of the models might be because volatile emissions of MEA were not included in the model. Moser et al. (2020) reported an MEA emission below 3 mg/m^3 in the modelled period. If these emissions were included in the model, an additional 14 kg of MEA would be lost, which would result in more precise models. This calculation can be found in Equation A.1 in Section A.3 in the Appendix. Another reason for the under-prediction might be the assumption of constant absorber temperature at 40 °C. Just a tiny increase in the absorber temperature would increase oxidative degradation significantly. This is especially the case for the advanced model, which will be shown in the following Section.

The Niederaussem pilot plant is different from other plants which have measured MEA degradation. Most of the other published articles on pilot plants have a specific MEA degradation between 1.5-3.5 kg MEA per ton CO_2, far more than what was observed at Niederaussem[10]. Both models did predict relatively close solvent losses compared to the pilot plant.

4.4 Full Scale CO_2-capture Plants

In this section, the two industrial scaled CO_2 capture plants are compared. The first case is from a typical 400 MW coal-based power plant, and the second is from a typical 400 MW Natural Gas (NG)-based power plant.

The process conditions of the two cases can be seen in Figure A.3. First, results from the simulation showing the optimal L/G ratio and temperature profiles in the absorber column will be shown in Section 4.4.1. Then, the degradation models are applied to the two cases in Section 4.4.2. The flue gas flow rate was constant for both studies while having a CO_2-capture rate of 90%. The study of coal flue gas is often referred as just coal, and the study with the natural gas flue gas is called NG.

4.4.1 Simulation of Full Scale CO_2-capture Plants

The simulation results for the coal and NG industrial cases can be found in Table A.4 and A.5, respectively, in the Appendix, Section A.4. For the coal study, the L/G ratio varied between 2.0 and 7.0, while it ranged between 0.75 and 4.0 for NG. The specific energy consumption (GJ/t_{CO_2}) are plotted against the L/G ratio for coal and NG in Figure 4.7.

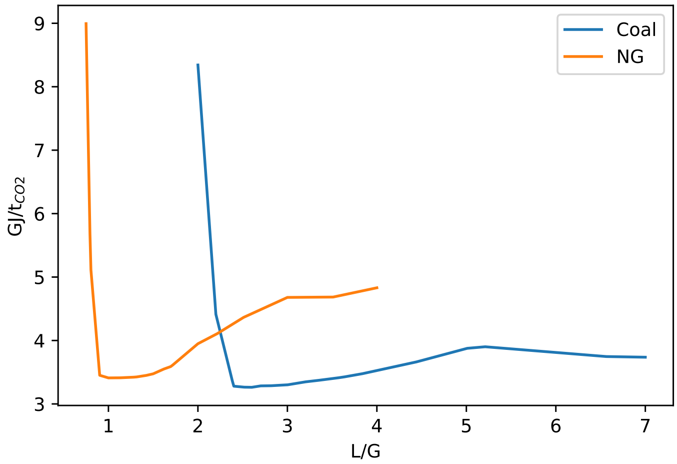

Figure 4.7: Energy demand in reboiler per ton CO_2- captured for different L/G values for coal (blue) and NG (orange).

With flue gas from coal, shown as the blue line in Figure 4.7, it can be seen that the reboiler duty is massive when the L/G ratio is lower than 2.5. If the L/G were to increase from 2.5, it looks like a linear increase in the reboiler duty. Then, the specific energy consumption decreases because of a sudden hop in the lean loading, as shown in Figure 4.8a. These simulations found an optimal L/G ratio concerning energy demand to be 2.6 for the coal case. At this L/G, the lean loading was 0.17, the rich loading was 0.52, and the reboiler duty was 286 MW, seen in Table A.4. At this L/G, the specific energy consumption is 3.26 GJ/t_{CO_2}.

The specific energy consumption for NG is shown as orange in Figure 4.7 for L/G ranging between 0.75 and 4.0. It can be observed a similar trend as for coal. Although, the optimal L/G ratio was here 1.1. It was expected to be lower than coal due to the lower CO_2 concentration in the flue gas. Table A.5 shows that the lean loading was 0.21 and the rich loading was 0.50, with a reboiler duty operating at 152 MW. The specific energy consumption at the energy optimal L/G is here 3.41 GJ/t_{CO_2}.

Equation 2.25 in Section 2.3 can be used to describe Figure 4.7. The last term in this equation is causing the exponential increase in energy for lower L/G. This term is increasing because the desorption driving forces are becoming small with the low partial pressure of CO_2[39]. Therefore, this last part of the equation is exponentially increased with the massive increase in required water vapour pressure. The first term in the equation represents the heat of CO_2-desorption, which was constant in all simulations as the capture rate and flue gas flow rate were constant. The middle term of the equation can be used to describe the behaviour of the slow linear increase in reboiler duty after the optimal L/G, observed in Figure 4.7. This is because more solvent must be heated as the L/G ratio increases. Figure 4.8 shows the lean and rich loading plotted against the L/G ratio for coal (4.8a) and NG (4.8b). The lean loading are in both cases illustrated as a blue line, while the rich loading is shown as red.

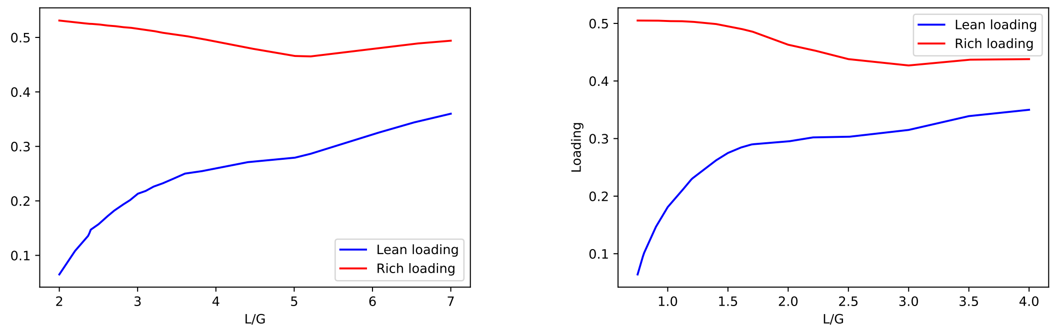

(a) **Coal** (b) **NG**

Figure 4.8: Lean and rich loading in the simulations with coal and NG flue gas for different L/G values.

Figure 4.8a shows that the lean loading for coal increases rapidly when the L/G ratio is increased from 2.0 to 4.0. The lean loading flattens out to some extent before it linearly increases from an L/G of 5.0. The rich loading decreases linearly to 0.47, then increases to 0.49 when L/G is 7.0. The cyclic loading capacity(α_{rich}-α_{lean}) was, however, decreased as the L/G ratio increased, as expected. This decrease was expected because the higher the flow rate of the solvent and with constant amount of CO_2 absorbed, the fewer MEA molecules could react and carry CO_2. It can be seen that the energy consumption also went down with the sudden increase in lean loading at L/G = 5.0. This can be seen as the blue line decreasing at L/G = 5.0 in Figure 4.7. This illustrates that the energy needed to strip to a lower loading is more significant than the energy required to heat a larger fraction of the solvent to the stripping temperature.

Figure 4.8b shows the lean and rich loading for the NG simulations. Like coal, it starts with an initial large increase in the lean loading while the rich loading decreases slowly. The growth in the lean loading stagnates near an L/G of 1.5, where the rich loading starts to decrease at a higher rate. A sudden increase in the rich loading is also found in the NG simulations, here when L/G is 3.0. The cyclic loading capacity is also here decreasing with higher L/G ratios.

The simulations that yielded the optimal L/G ratio regarding energy consumption in the reboiler were chosen for a degradation study. Temperature profiles in the absorber for these runs can be seen in Figure 4.9, for coal and NG.

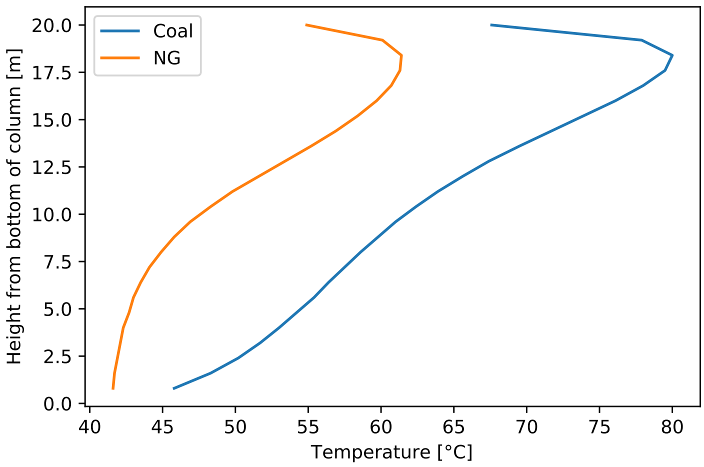

Figure 4.9: Temperature profiles in the absorber column for coal (blue) and NG (orange) with optimal L/G concerning the energy demand.

Figure 4.9 shows that there is a significant temperature difference in the absorber between the two cases. The solvent was in both cases inserted in the column at 40 °C. For the simulation with coal, the temperature was instantaneously increased to 80 °C, while for NG, the solvent temperature increased to 61 °C initially. With the assumption of constant liquid flow, an average temperature was found to be 63.4 and 50.1 °C, respectively, for coal and NG. The temperature bulge is for both cases located near the top of the column, or 16-18 meters from the bottom of the column. This shows that most of the absorption happened at the top of the column, due to the exothermic absorption releasing heat.

Using the average temperature like this might result in an underestimation of the oxidative degradation. This is because the reaction rate of oxidative degradation is an exponential function with regard to temperature. The rate of oxidative degradation would be significantly higher at the maximum temperature than the average temperature calculated here. Optimally, it should have been integrated over the column and calculated the oxidative degradation in each section.

It was expected that the temperature in the absorber with coal flue gas was higher than for NG as the CO_2 content is significantly higher in coal flue gases. This temperature difference might indicate that the degradation rate is higher for coal flue gases, as oxidative degradation highly depends on the absorber temperature. The oxygen concentration is, however, larger for NG, which also gives more oxidative degradation.

Figure 4.7 showed no reason to use a carbon capture plant that uses a lower L/G value than the optimal one, as the reboiler energy demand would be massive. The cost of the large increase in reboiler duty would be severe. However, by increasing the L/G ratio, there was just observed a minor increase in the reboiler duty. Having a larger L/G might change the temperature profiles profitably regarding degradation. The maximum and average temperature in the column would be lower, meaning less degradation. Therefore, an MEA consumption study will also be done in the next section when the L/G is higher than the obtained optimal ones.

4.4.2 Degradation in Full Scale CO_2-capture Plants

The two cases with optimal L/G concerning energy consumption in the reboiler are here compared considering degradation. Both instances are modelled over 25 weeks, where the MEA consumption and accumulation of degradation products are compared. The initial MEA concentration is 4.91 mol/L. Both the simplified model and the advanced model are used in both cases, seen in Figure 4.10.

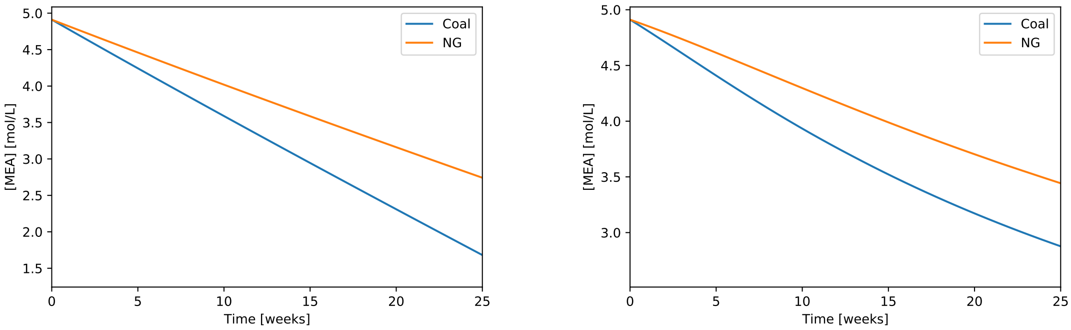

(a) Simplified model **(b) Advanced model**

Figure 4.10: MEA consumption for coal and NG with the simplified model (4.10a) and the advanced model(4.10b).

The simplified model predicts an MEA concentration of 1.7 mol/L after 25 weeks for coal. With NG, the end concentration of MEA is 2.8 mol/L. The advanced model predicts an MEA concentration of 2.9 mol/L for coal, and 3.5 mol/L for NG. Both models predict more degradation for coal than NG. Table 4.2 shows the change in MEA concentration, solvent volume, amount of CO_2 captured, the mass of degraded MEA and the specific MEA consumption for both cases with both degradation models. The amount of captured CO_2 comes from the simulation in ProTreat, or seen as 90% of the CO_2 which is sent to the absorber after 25 weeks. The solvent volumes were assumed in Section 3.5.1.

Table 4.2: Specific MEA consumption for coal and NG measured by both models when the L/G ratio is at an energy optimal.

	Simplified model		Advanced model	
	Coal	NG	Coal	NG
Δ C_{MEA} [mol/L]	3.21	2.16	2.01	1.46
Solvent volume [m^3]	3737	1903	3737	1903
CO_2 captured [ton]	1325234	674062	1325234	674062
MEA degraded [kg]	732733	251040	458814	169684
MEA consumption [kg MEA/t_{CO_2}]	0.553	0.372	0.346	0.252

It can be seen in Table 4.2, even though the case with coal captures more CO_2 than NG, that the specific MEA consumption is still larger for coal. The larger oxygen content in the flue gas from NG does not seem to cause a significant increase in the solvent degradation. The simplified model predicts a specific MEA consumption of 0.55 and 0.37 kg MEA/t_{CO_2} for coal and NG, respectively. The advanced model predicts a specific MEA consumption of 0.37 and 0.25 kg MEA/t_{CO_2} for coal and NG, respectively. Equation A.2 in Section A.3 in the Appendix shows how the amount of total MEA degraded was calculated. One way to reduce degradation is by lowering the temperatures, especially in the absorber column. If the L/G ratio is increased, there is more liquid to absorb the heat from the heat of reaction of CO_2 with the amines. In addition, the lean loading is expected to increase, resulting in a lower temperature in the reboiler. A lower temperature in the reboiler means less thermal degradation. However, even though the temperature is decreased, the higher lean loading will result in more CO_2, which can react with MEA causing thermal degradation. To investigate this, L/G ratios of 7.0 and 4.0 were chosen for the coal and NG study, respectively. There is only a 14% larger reboiler duty when L/G is 7.0 instead of the optimal one at 2.6 for the coal study. For NG, the reboiler duty is 42% larger by having an L/G of 4.0 instead of 1.1. The temperature profiles for the simulations with the increased L/G can be seen in Figure 4.11.

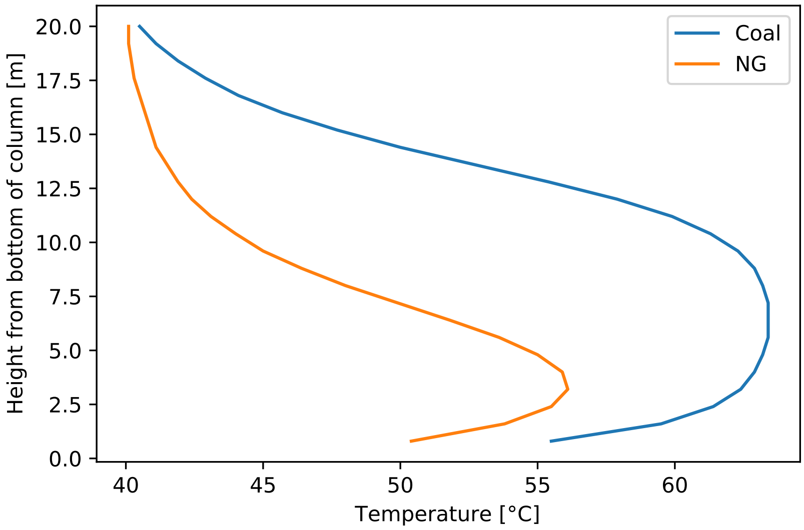

Figure 4.11: Temperature profiles in the absorber column for coal (blue) and NG (orange) for high L/G ratios.

A clear difference can be found by comparing the temperature profiles with high L/G in Figure 4.11 with the energy optimal ones in Figure 4.9. First of all, the temperature bulges are now near the bottom of the column. This was expected as more solvent can reach the bottom of the column before becoming saturated with CO_2. Furthermore, it can be seen that the overall temperatures are lower. That was also expected as the same amount of CO_2 is reacting while the solvent flow is larger. The average temperature in the coal simulation is now 55.4 °C, down from 63.4 °C, which was the average temperature with the optimal L/G. For NG, the average temperature decreased from 50.1 to 46.3 °C by increasing the L/G from 1.1 to 4.0. Figure 4.12 shows the MEA consumption for both cases predicted by the simplified model (4.12a) and the advanced model (4.12b) when the L/G ratios are high.

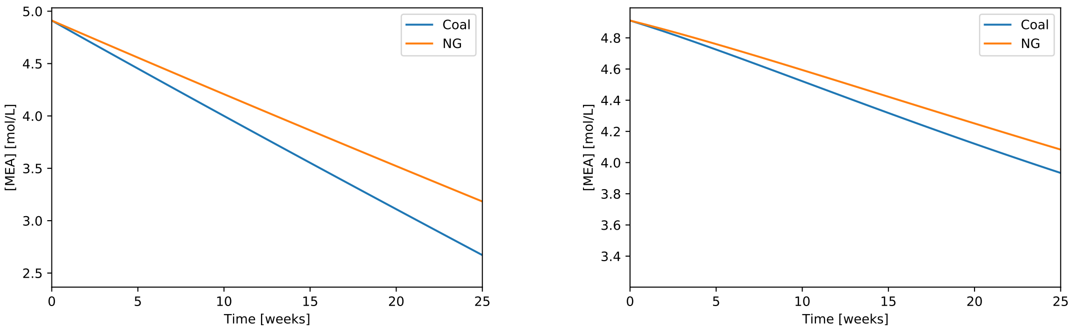

(a) Simplified model **(b) Advanced model**

Figure 4.12: MEA consumption for coal and NG with the simplified model (4.12a) and the advanced (4.12b) when the L/G value is 7.0 and 4.0 for coal and NG, respectively.

It can be seen from Figure 4.12 that there is still a greater degradation rate for coal. Comparing these two figures with the MEA consumption with optimal L/G seen in Figure 4.2, a relatively larger gap between the two cases can be seen in the simplified model. The advanced model predicts a more similar degradation rate for the cases with large L/G. The main reason for the more similar degradation rates in the advanced model might be that it is more sensitive to temperature in the absorber. For the coal study, the absorber temperature was decreased by 8 °C when the L/G was increased from 2.6 to 7.0. This is twice the temperature decrease as was observed for NG. The average temperature decreased by 4 °C when the L/G ratio was increased from 1.1 to 4.0 for NG.

In addition to a lower temperature in the absorber, the reboiler temperature were in both cases decreased to 113 °C. This temperature decrease reduces the thermal degradation significantly. Overall, the degradation rate is lower than the cases with optimal L/G ratio concerning energy, as expected. The specific energy consumption can be found in Table 4.3.

Table 4.3: Specific MEA consumption for coal and NG measured by both models when the L/G ratio is high.

	Simplified model		Advanced model	
	Coal	NG	Coal	NG
Δ C_{MEA} [mol/L]	2.24	1.73	0.96	0.81
Solvent volume [m^3]	3737	1903	3737	1903
CO_2 captured [ton]	1325234	674062	1325234	674062
MEA degraded [kg]	511293	201086	219125	94150
MEA consumption [kg MEA/t_{CO_2}]	0.386	0.298	0.165	0.140

Table 4.3 shows that by increasing the L/G ratio, the specific MEA consumption reduces significantly. Increasing the L/G ratio means a lower temperature in the absorber and lower reboiler temperature as the stripper can strip to higher lean loading. However, the reboiler duty increases, and so does the pumps' energy consumption. Before a conclusion on which L/G is the most beneficial, an economic study must be done.

In the last part of this chapter, a degradation study is done with the advanced degradation model for the two cases with optimal L/G ratio concerning the reboiler energy demand. Figure 4.13 shows the predicted accumulation of NH_3 (4.13a), HEF (4.13b), HEI (4.13c) and HEGly (4.13d) for coal and NG.

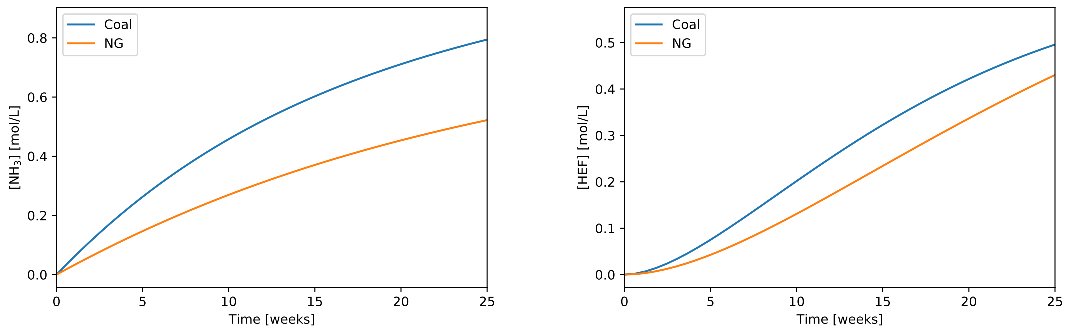

(a) $\mathbf{NH_3}$ **(b) HEF**

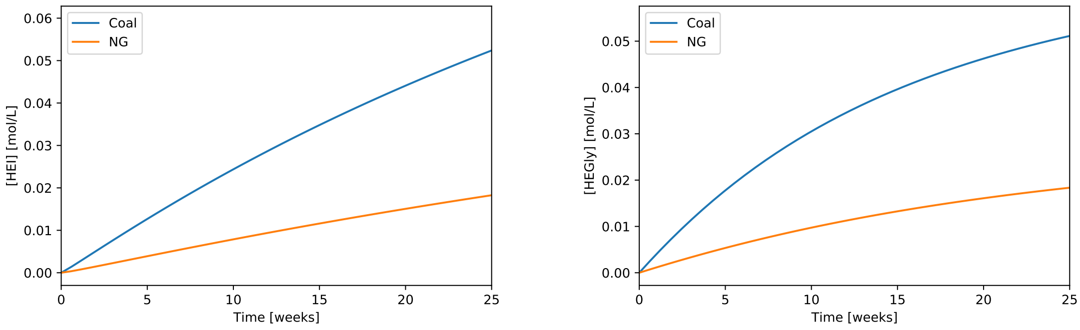

(c) HEI **(d) HEGly**

Figure 4.13: The advanced model's prediction on $\mathbf{NH_3}$ (4.13a), HEF (4.13b), HEI (4.13c) and HEGly (4.13d) on the coal case (blue) and the NG case (orange).

When comparing the degradation products between coal and NG, it can be found which compound is more dependent on oxygen and which is more dependent on temperature in the oxidative model.

For instance, the formation of HEF, seen in Figure 4.13b, seems quite similar for both cases. This can indicate that the formation of HEF is not as dependent on temperature compared to other compounds. It might look like the concentration of HEF for coal is flattening out while a linear increase is observed for NG near the end weeks. HEF is formed from Equation 2.13 where protonated MEA reacts with formate. Formate is assumed to have the same concentration as formic acid produced by oxidation of formaldehyde, seen in Equation 2.12. Since the concentration of formic acid, seen in Figure 4.14a, is over twice as high for coal than it is for NG, it means that the formation of HEF depends less on temperature.

HEGly and HEI, seen in Figure 4.13d and 4.13c, seem to be more favourable by high temperatures, as the concentration of these products is significantly higher for the coal case. The rapid increase in HEGly concentration with increasing temperature was also found in the oxidative degradation study by Vevelstad et al. (2014). Léonard et al. (2014) found a considerable increase of HEI when increasing the temperature in a solvent degradation experiment[56]. This behaviour was also observed here, as the concentrations of HEGly and HEI were increasing when the fuel was coal with a higher absorber temperature. The ammonia formation seen in Figure 4.13a seems to be somewhere in the middle. The relative concentration gap is larger than HEF but smaller than HEI and HEGly[15].

Figure 4.14 shows the formation of formic acid (4.14a), formaldehyde (4.14b), HEEDA (4.14c) and HEIA (4.14d) for coal and NG.

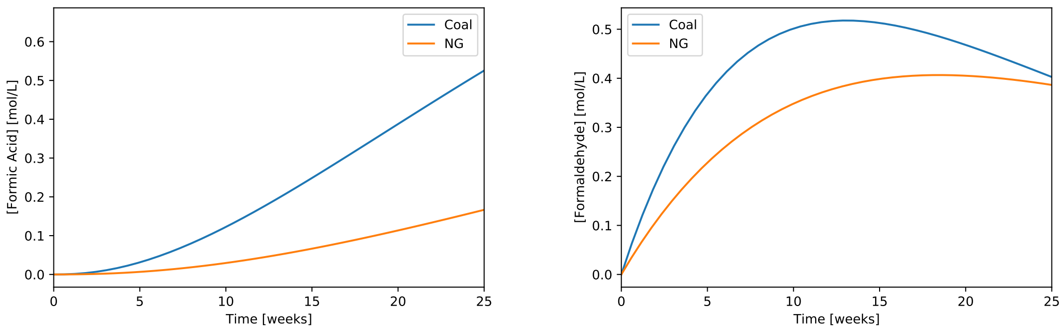

(a) Formic acid **(b) Formaldehyde**

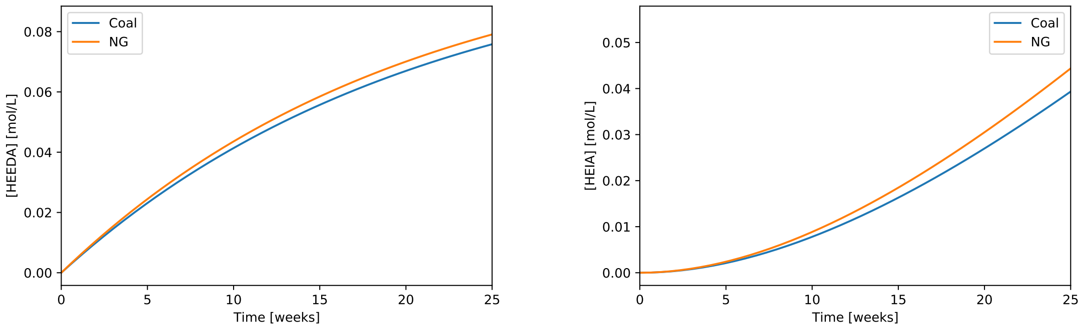

(c) HEEDA **(d) HEIA**

Figure 4.14: The advanced model's prediction on formic acid (4.14a), formaldehyde (4.14b), HEEDA (4.14c) and HEIA (4.14d) for coal (blue) and NG (orange) with optimal L/G ratio.

Figure 4.14a shows that the formation of formic acid is over twice as large after 25 weeks for the coal case. This indicates that the reaction in Equation 2.12 strongly depends on the temperature. The reason for the more similar HEF formation between the two cases can therefore be described by Equation 2.13, which is not very affected by temperature. More formaldehyde is produced for coal initially, but it looks like the formaldehyde concentration is larger for NG after 25 weeks of operation.

The thermal degradation compounds HEEDA and HEIA, seen in Figure 4.14c and 4.14d, show that the NG plant has the most thermal degradation. More thermal degradation in NG can be seen even though the reboiler temperature was 1 °C lower than for coal. This is because NG has a higher lean loading than coal. NG had a lean loading of 0.21, while coal had a loading of 0.17. In this model, the most considerable portion of the volume exposed to high temperatures has a lean loading, which is why NG has more thermal degradation than coal. It looks like HEEDA in both cases stagnates near 0.08 mol/L while the concentration of HEIA is continuously growing and will, after additional time, be more concentrated than HEEDA. This trend was expected as HEIA was proposed to be an end product while HEEDA being the intermediate in the reaction.

Overall, it looks like this model is predicting most degradation for coal-based power plants because of a larger temperature in the absorber. This increased absorber temperature is the result of a higher CO_2 concentration in the flue gas. Even though the oxygen content of flue gases emitted by NG-based power plants is higher, the degradation rate is still lower.

In previous pilot-scale pilot plants, the major degradation products have varied[31]. In a pilot plant at Longannet using coal flue gas, the most significant degradation compound was HEF. Too little analytical data are available from this pilot plant to draw any conclusions as to why HEF was so significant[31]. The large formation of HEF is however one similarity to the advanced degradation model in this work. From pilot plants at Tiller and Esbjerg, the results were different[31]. The most significant degradation compound at the Esbjerg pilot plant was HEGly. The following compound was HEPO. In the Tiller pilot plant, HEPO was the most concentrated and HEGly was the second most concentrated.

Since the degradation rate has varied in other pilot plants[16][10][31], it is difficult to validate the predicted degradation on the industrial-scale, which has been done in this work. Even though the models fit quite well with the lab-scale experiment, the industrial case study were modelled over a significant longer period. This indicates more uncertainties.

CHAPTER 5

CONCLUSION

The degradation models were developed and implemented in Python and used to predict solvent degradation. The model predictions were compared to both lab-scale and pilot-scale data and were used to model degradation in two industrial cases with natural gas and coal-based flue gases.

The simple degradation model is based on an oxidative degradation study conducted by Vevelstad et al. (2014), an in-house thermal degradation model at NTNU and degradation from impurities based on a study by Rao et al. (2002). The oxidative degradation equation for this simplified model was fitted in this work.

The advanced degradation model is based on reaction rates obtained by Pinto et al. (2014), another in-house thermal degradation model, and degradation from impurities based on the study by Rao et al. (2002). Parameters used in this model were fitted in previous work.

The MEA consumption of the lab-scale experiment was predicted by both models, where the advanced model fits quite well. The simplified model over-predicted the MEA consumption to some extent. The advanced degradation model was further used to predict the accumulated degradation compounds in the liquid phase in the experiment. Here it was found that the model over-predicts the compounds which are volatile, like ammonia and formaldehyde. This over-predicting is most likely because the model does not include evaporation of the degradation products. This might have caused a larger degradation rate of other compounds since both ammonia and formaldehyde were proposed as intermediates. However, the model predicts the concentration of HEI, formic acid, HEEDA and HEIA relatively well. The compound that deviated the most was HEF.

The oxidative degradation model is based on a purely oxidative study. Since the degradation products depend on each other, the reactions occurring in the desorber will influence the reactions occurring in the absorber and vice versa. HEGly and HEPO are primarily affected by this. HEGly is in the model proposed as an end product, while previous studies show that it is an intermediate forming HEPO at elevated temperatures. HEPO was not included in the model but might have been one of the major degradation products.

The simplified model fits best when applied at the process conditions of the pilot-scale plant. The specific MEA consumption predicted by the simplified model was 0.24 kg MEA/t_{CO_2}, close to the observed MEA consumption at the pilot plant, being below 0.3 kg MEA/t_{CO_2}. The advanced model, however, predicted an MEA consumption of 0.13 kg MEA/t_{CO_2}.

In the industrial case study, two different flue gases were used for simulations and degradation studies. The first flue gas came from a typical 400 MW coal-based power plant, while the other from a 400 MW natural gas-based power plant. Simulations in ProTreat were done with the flue gases with flow rates and gas compositions based on literature while varying the Liquid-to-Gas (L/G) ratio. The optimal L/G ratio concerning energy consumption in the reboiler was 2.6 and 1.1 for coal and natural gas, respectively. At these L/G ratios, a specific energy consumption was calculated to be 3.26 and 3.41 GJ/t_{CO_2} for coal and natural gas, respectively. The specific MEA consumption [kg MEA/t_{CO_2}] was for both degradation models higher for coal. Even though the oxygen content from a natural gas-based power plant is higher, solvent degradation is still lower than for the coal-based power plant. This is mainly because of the higher absorber temperature with the more CO_2-concentrated flue gas from coal.

A significant decrease in solvent degradation was found by having a higher L/G ratio than the optimal one considering energy consumption. This decrease in degradation occurred because of a lower absorber temperature. In addition, the reboiler temperature was also lower for the higher L/G ratio, which decreased the thermal degradation.

CHAPTER 6

FURTHER RECOMMENDATIONS

The models developed in this work should be further improved. One could start by fitting the advanced oxidative model with the oxygen solubility model, which includes the effect of solvent loading. Rate equations describing oxidative and thermal should ideally be fit from several experiments where the absorber and desorber are connected. By doing this, compounds like HEPO and HEGly can be modelled more precisely.

Furthermore, the model should include the volatile emissions of MEA, NH_3 and formaldehyde. Aerosol emissions is another contribution to the overall solvent loss which should be included. The effect of dissolved metals should be further investigated and be included in the model.

In order to estimate a more precise oxidative degradation, one should integrate over the absorber column. This way, the correct temperature in each section is used to calculate the rate of reactions. This is important as the oxidative degradation increases exponentially with the absorber temperature. The same approach can be used on the desorber column to get a more precise rate of thermal degradation. The contribution of dissolved oxygen in the rich solvent stream on the degradation was not considered and should be included in the model.

Once a new and more advanced model is developed, it should be validated on several lab-scale and pilot-scale campaigns.

Lastly, the impact of the different degradation product should be investigated. Doing this makes it easier to control the emissions of the worst ones and potentially reduce them.

BIBLIOGRAPHY

[1] Raili Kajaste and Markku Hurme. Cement industry greenhouse gas emissions – management options and abatement cost. *Journal of Cleaner Production*, 112:4041–4052, 2016. ISSN 0959-6526. doi: https://doi.org/10.1016/j.jclepro.2015.07.055. URL `https://www.sciencedirect.com/science/article/pii/S095965261500983X`.

[2] Kevin E. Trenberth and John T. Fasullo. Global warming due to increasing absorbed solar radiation. *Geophysical Research Letters*, 36(7). doi: https://doi.org/10.1029/2009GL037527. URL `https://agupubs.onlinelibrary.wiley.com/doi/abs/10.1029/2009GL037527`.

[3] Qingchen Chao and Aiqing Feng. Scientific basis of climate change and its response. *Global Energy Interconnection*, 1(4):420–427, 2018. ISSN 2096-5117. doi: https://doi.org/10.14171/j.2096-5117.gei.2018.04.002. URL `https://www.sciencedirect.com/science/article/pii/S2096511718300628`.

[4] The Intergovernmental Panel on Climate Change. AR5 Climate Change 2014: Mitigation of Climate Change, 2014. URL `https://www.ipcc.ch/report/ar5/wg3/`.

[5] Yujiong Gu, Jing Xu, Dongchao Chen, Zhong Wang, and Qianqian Li. Overall review of peak shaving for coal-fired power units in China. *Renewable and Sustainable Energy Reviews*, 54:723–731, 2016. ISSN 1364-0321. doi: https://doi.org/10.1016/j.rser.2015.10.052. URL `https://www.sciencedirect.com/science/article/pii/S1364032115011314`.

[6] Yuan Wang, Li Zhao, Alexander Otto, Martin Robinius, and Detlef Stolten. A Review of Post-combustion CO2 Capture Technologies from Coal-fired Power Plants. *Energy Procedia*, 114: 650–665, 2017. ISSN 1876-6102. doi: https://doi.org/10.1016/j.egypro.2017.03.1209. URL `https://www.sciencedirect.com/science/article/pii/S1876610217313851`. 13th International Conference on Greenhouse Gas Control Technologies, GHGT-13, 14-18 November 2016, Lausanne, Switzerland.

[7] Volker Roeder and Alfons Kather. Part Load Behaviour of Power Plants with a Retrofitted Post-combustion CO2 Capture Process. *Energy Procedia*, 51:207–216, 2014. ISSN 1876-6102. doi: https://doi.org/10.1016/j.egypro.2014.07.024. URL `https://www.sciencedirect.com/science/article/pii/S1876610214008868`. 7th Trondheim Conference on CO2 capture, Transport and Storage (2013).

[8] Liv-Margrethe Bjerge and Per Brevik. CO2 Capture in the Cement Industry, Norcem CO2 Capture Project (Norway). *Energy Procedia*, 63:6455–6463, 2014. ISSN 1876-6102. doi: https://doi.org/10.1016/j.egypro.2014.11.680. URL `https://www.sciencedirect.com/science/article/pii/S1876610214024953`. 12th International Conference on Greenhouse Gas Control Technologies, GHGT-12.

[9] Chunshan Song, Wei Pan, Srinivas T. Srimat, Jian Zheng, Yan Li, Yu-He Wang, Bo-Qing Xu, and Qi-Ming Zhu. Tri-reforming of Methane over Ni Catalysts for CO2 Conversion to Syngas With Desired H2/CO Ratios Using Flue Gas of Power Plants Without CO2 Separation. In Sang-Eon Park, Jong-San Chang, and Kyu-Wan Lee, editors, *Carbon Dioxide Utilization for Global Sustainability*, volume 153 of *Studies in Surface Science and Catalysis*, pages 315–322. Elsevier, 2004. doi: https://doi.org/10.1016/S0167-2991(04)80270-2. URL `https://www.sciencedirect.com/science/article/pii/S0167299104802702`.

[10] Peter Moser, Georg Wiechers, Sandra Schmidt, Juliana Garcia Moretz-Sohn Monteiro, Charithea Charalambous, Susana Garcia, and Eva Sanchez Fernandez. Results of the 18-month test with MEA at the post-combustion capture pilot plant at Niederaussem – new impetus to solvent management, emissions and dynamic behaviour. *International Journal of Greenhouse Gas Control*, 95:102945, 2020. ISSN 1750-5836. doi: https://doi.org/10.1016/j.ijggc.2019.102945. URL `https://www.sciencedirect.com/science/article/pii/S1750583619306371`.

[11] D Singh, E Croiset, P.L Douglas, and M.A Douglas. Techno-economic study of CO2 capture from an existing coal-fired power plant: MEA scrubbing vs. O2/CO2 recycle combustion. *Energy Conversion and Management*, 44(19):3073–3091, 2003. ISSN 0196-8904. doi: https://doi.org/10.1016/S0196-8904(03)00040-2. URL `https://www.sciencedirect.com/science/article/pii/S0196890403000402`.

[12] Nina Enaasen Flø, Leila Faramarzi, Thomas de Cazenove, Odd Arne Hvidsten, Anne Kolstad Morken, Espen Steinseth Hamborg, Kai Vernstad, Guillaume Watson, Steinar Pedersen, Toine Cents, Berit F. Fostås, Muhammad Ismail Shah, Gerard Lombardo, and Erik Gjernes. Results from MEA Degradation and Reclaiming Processes at the CO2 Technology Centre Mongstad. *Energy Procedia*, 114:1307–1324, 2017. ISSN 1876-6102. doi: https://doi.org/10.1016/j.egypro.2017.03.1899. URL `https://www.sciencedirect.com/science/`

`article/pii/S1876610217321021`. 13th International Conference on Greenhouse Gas Control Technologies, GHGT-13, 14-18 November 2016, Lausanne, Switzerland.

[13] Mohammad R.M. Abu-Zahra, Léon H.J. Schneiders, John P.M. Niederer, Paul H.M. Feron, and Geert F. Versteeg. CO2 capture from power plants: Part I. A parametric study of the technical performance based on monoethanolamine. *International Journal of Greenhouse Gas Control*, 1(1):37–46, 2007. ISSN 1750-5836. doi: https://doi.org/10.1016/S1750-5836(06)00007-7. URL `https://www.sciencedirect.com/science/article/pii/S1750583606000077`. 8th International Conference on Greenhouse Gas Control Technologies.

[14] Grégoire Léonard, Alexander Voice, Dominique Toye, and Georges Heyen. Influence of Dissolved Metals and Oxidative Degradation Inhibitors on the Oxidative and Thermal Degradation of Monoethanolamine in Postcombustion CO2 Capture. *Industrial & Engineering Chemistry Research*, 53(47):18121–18129, 2014. doi: 10.1021/ie5036572. URL `https://doi.org/10.1021/ie5036572`.

[15] Solrun Johanne Vevelstad, Maren T. Johansen, Hanna Knuutila, and Hallvard F. Svendsen. Oxygen and Temperature Effect on Formation of Degradation Compounds from MEA. *Energy Procedia*, 63:957–975, 2014. ISSN 1876-6102. doi: https://doi.org/10.1016/j.egypro.2014.11.105. URL `https://www.sciencedirect.com/science/article/pii/S1876610214019201`. 12th International Conference on Greenhouse Gas Control Technologies, GHGT-12.

[16] Vanja Buvik, Karen K. Høisæter, Sorun J. Vevelstad, and Hanna K. Knuutila. A review of degradation and emissions in post-combustion CO2 capture pilot plants. *International Journal of Greenhouse Gas Control*, 106:103246, 2021. ISSN 1750-5836. doi: https://doi.org/10.1016/j.ijggc.2020.103246. URL `https://www.sciencedirect.com/science/article/pii/S175058362030671X`.

[17] Karin Veltman, Bhawna Singh, and Edgar G. Hertwich. Human and Environmental Impact Assessment of Postcombustion CO2 Capture Focusing on Emissions from Amine-Based Scrubbing Solvents to Air. *Environmental Science & Technology*, 44(4):1496–1502, 2010. doi: 10.1021/es902116r. URL `https://doi.org/10.1021/es902116r`. PMID: 20095561.

[18] Zhe Lun Ooi, Pui Yee Tan, Lian See Tan, and Swee Pin Yeap. Amine-based solvent for CO2 absorption and its impact on carbon steel corrosion: A perspective review. *Chinese Journal of Chemical Engineering*, 28(5):1357–1367, 2020. ISSN 1004-9541. doi: https://doi.org/10.1016/j.cjche.2020.02.029. URL `https://www.sciencedirect.com/science/article/pii/S1004954120301002`.

[19] Bhurisa Thitakamol, Amornvadee Veawab, and Adisorn Aroonwilas. Foaming in amine-based CO2 capture process: Experiment, modeling and simulation. *Energy Procedia*, 1(1):1381–1386, 2009. ISSN 1876-6102. doi: https://doi.org/10.1016/j.egypro.2009.01.181. URL `https:`

//www.sciencedirect.com/science/article/pii/S1876610209001829. Greenhouse Gas Control Technologies 9.

[20] Maximilian Biermann, Fredrik Normann, Filip Johnsson, and Ragnhild Skagestad. Partial Carbon Capture by Absorption Cycle for Reduced Specific Capture Cost. *Industrial & Engineering Chemistry Research*, 57(45):15411–15422, 2018. doi: 10.1021/acs.iecr.8b02074. URL `https://doi.org/10.1021/acs.iecr.8b02074`.

[21] Wolfgang Sanz, M Mayr, and H Jericha. Thermodynamic and Economic Evaluation of an IGCC Plant Based on the Graz Cycle for CO2 Capture. *Proceedings of the ASME Turbo Expo*, 3, 10 2010. doi: 10.1115/GT2010-22189.

[22] Ernst A. van Nierop, Sahand Hormoz, Kurt Z. House, and Michael J. Aziz. Effect of absorption enthalpy on temperature-swing CO2 separation process performance. *Energy Procedia*, 4:1783–1790, 2011. ISSN 1876-6102. doi: https://doi.org/10.1016/j.egypro.2011.02.054. URL `https://www.sciencedirect.com/science/article/pii/S1876610211002517`. 10th International Conference on Greenhouse Gas Control Technologies.

[23] Bihong Lv, Bingsong Guo, Zuoming Zhou, and Guohua Jing. Mechanisms of CO2 Capture into Monoethanolamine Solution with Different CO2 Loading during the Absorption/Desorption Processes. *Environmental Science & Technology*, 49(17):10728–10735, 2015. doi: 10.1021/acs.est.5b02356. URL `https://doi.org/10.1021/acs.est.5b02356`. PMID: 26236921.

[24] G. Puxty and M. Maeder. 2 - The fundamentals of post-combustion capture. In Paul H.M. Feron, editor, *Absorption-Based Post-combustion Capture of Carbon Dioxide*, pages 13–33. Woodhead Publishing, 2016. ISBN 978-0-08-100514-9. doi: https://doi.org/10.1016/B978-0-08-100514-9.00002-0. URL `https://www.sciencedirect.com/science/article/pii/B9780081005149000020`.

[25] Anand B. Rao and Edward S. Rubin. A Technical, Economic, and Environmental Assessment of Amine-Based CO2 Capture Technology for Power Plant Greenhouse Gas Control. *Environmental Science & Technology*, 36(20):4467–4475, 2002. doi: 10.1021/es0158861. URL `https://doi.org/10.1021/es0158861`. PMID: 12387425.

[26] Spietz, Chowola, Krótki, Tatarczuk, Wieclaw-Solny, and Wilk. Ammonia emission from CO2 capture pilot plant using aminoethylethanolamine. *International Journal of Environmental Science and Technology*, 15:1085–1092, 2018. doi: https://doi.org/10.1007/s13762-017-1475-z. URL `https://link.springer.com/article/10.1007/s13762-017-1475-z#citeas`.

[27] Alicia J. Reynolds, T. Vincent Verheyen, Samuel B. Adeloju, Erik Meuleman, and Paul Feron. Towards Commercial Scale Postcombustion Capture of CO2 with Monoethanolamine Solvent: Key Considerations for Solvent Management and Environmental Impacts. *Environmental*

Science & Technology, 46(7):3643–3654, 2012. doi: 10.1021/es204051s. URL `https://doi.org/10.1021/es204051s`. PMID: 22324566.

[28] Alexander Rieder, Sanjana Dhingra, Purvil Khakharia, Luigi Zangrilli, Bernd Schallert, Robin Irons, Sven Unterberger, Peter van Os, and Earl Goetheer. Understanding Solvent Degradation: A Study from Three Different Pilot Plants within the OCTAVIUS Project. *Energy Procedia*, 114:1195–1209, 2017. ISSN 1876-6102. doi: https://doi.org/10.1016/j.egypro.2017.03.1376. URL `https://www.sciencedirect.com/science/article/pii/S1876610217315618`. 13th International Conference on Greenhouse Gas Control Technologies, GHGT-13, 14-18 November 2016, Lausanne, Switzerland.

[29] Vanja Buvik, Ida M. Bernhardsen, Roberta V. Figueiredo, Solrun J. Vevelstad, Earl Goetheer, Peter van Os, and Hanna K. Knuutila. Measurement and prediction of oxygen solubility in post-combustion CO2 capture solvents. *International Journal of Greenhouse Gas Control*, 104:103205, 2021. ISSN 1750-5836. doi: https://doi.org/10.1016/j.ijggc.2020.103205. URL `https://www.sciencedirect.com/science/article/pii/S1750583620306307`.

[30] Diego D.D. Pinto, Thea W. Brodtkorb, Solrun J. Vevelstad, Hanna Knuutila, and Hallvard F. Svendsen. Modeling of Oxidative MEA Degradation. *Energy Procedia*, 63:940–950, 2014. ISSN 1876-6102. doi: https://doi.org/10.1016/j.egypro.2014.11.103. URL `https://www.sciencedirect.com/science/article/pii/S1876610214019183`. 12th International Conference on Greenhouse Gas Control Technologies, GHGT-12.

[31] Eirik F. da Silva, Hélène Lepaumier, Andreas Grimstvedt, Solrun Johanne Vevelstad, Aslak Einbu, Kai Vernstad, Hallvard F. Svendsen, and Kolbjørn Zahlsen. Understanding 2-Ethanolamine Degradation in Postcombustion CO2 Capture. *Industrial & Engineering Chemistry Research*, 51(41):13329–13338, 2012. doi: 10.1021/ie300718a. URL `https://doi.org/10.1021/ie300718a`.

[32] Grégoire Léonard, Cyril Crosset, Marie-Noëlle Dumont, and Dominique Toye. Designing Large-scale CO2 Capture Units with Assessment of Solvent Degradation. *Energy Procedia*, 63:1478–1486, 2014. ISSN 1876-6102. doi: https://doi.org/10.1016/j.egypro.2014.11.157. URL `https://www.sciencedirect.com/science/article/pii/S1876610214019729`. 12th International Conference on Greenhouse Gas Control Technologies, GHGT-12.

[33] George S. Goff and Gary T. Rochelle. Monoethanolamine Degradation: O2 Mass Transfer Effects under CO2 Capture Conditions. *Industrial & Engineering Chemistry Research*, 43(20):6400–6408, 2004. doi: 10.1021/ie0400245. URL `https://doi.org/10.1021/ie0400245`.

[34] C. Gouedard, D. Picq, F. Launay, and P.-L. Carrette. Amine degradation in CO2 capture. I. A review. *International Journal of Greenhouse Gas Control*, 10:244–270, 2012. ISSN 1750-

5836. doi: https://doi.org/10.1016/j.ijggc.2012.06.015. URL `https://www.sciencedirect.com/science/article/pii/S1750583612001508`.

[35] Bohak Yoon, Haley M. Stowe, and Gyeong S. Hwang. Molecular mechanisms for thermal degradation of CO2-loaded aqueous monoethanolamine solution: a first-principles study. *Phys. Chem. Chem. Phys.*, 21:22132–22139, 2019. doi: 10.1039/C9CP04518J. URL `http://dx.doi.org/10.1039/C9CP04518J`.

[36] Jason Daniel Davis. *Thermal Degradation of Aqueous Amines Used for Carbon Dioxide Capture*. PhD thesis, The University of Texas at Austin, 2009.

[37] Scottish Environment Protection Agency. Review of amine emissions from carbon capture systems, 2015. URL `https://www.sepa.org.uk/media/155585/review-of-amine-emissions-from-carbon-capture-systems.pdf`. Found: 31.03.2021.

[38] Kangkang Li, Wardhaugh Leigh, Paul Feron, Hai Yu, and Moses Tade. Systematic study of aqueous monoethanolamine (MEA)-based CO2 capture process: Techno-economic assessment of the MEA process and its improvements. *Applied Energy*, 165:648–659, 2016. ISSN 0306-2619. doi: https://doi.org/10.1016/j.apenergy.2015.12.109. URL `https://www.sciencedirect.com/science/article/pii/S0306261915016827`.

[39] Xu Zhang, Kaiyun Fu, Zhiwu Liang, Zhen Yang, Wichitpan Rongwong, and Yanqing Na. Experimental Studies of Regeneration Heat Duty for CO2 Desorption from Aqueous DETA Solution in a Randomly Packed Column. *Energy Procedia*, 63:1497–1503, 2014. ISSN 1876-6102. doi: https://doi.org/10.1016/j.egypro.2014.11.159. URL `https://www.sciencedirect.com/science/article/pii/S1876610214019742`. 12th International Conference on Greenhouse Gas Control Technologies, GHGT-12.

[40] SINTEF. Results from the SDR campaign. 2020. Not public yet.

[41] Aslak Einbu, Eirik DaSilva, Geir Haugen, Andreas Grimstvedt, Kristin Giske Lauritsen, Kolbjørn Zahlsen, and Terje Vassbotn. A new test rig for studies of degradation of CO2 absorption solvents at process conditions; comparison of test rig results and pilot plant data for degradation of MEA. *Energy Procedia*, 37:717–726, 2013. ISSN 1876-6102. doi: https://doi.org/10.1016/j.egypro.2013.05.160. URL `https://www.sciencedirect.com/science/article/pii/S1876610213001707`. GHGT-11 Proceedings of the 11th International Conference on Greenhouse Gas Control Technologies, 18-22 November 2012, Kyoto, Japan.

[42] S Weisenberger and A Schumpe. Estimation of gas solubilities in salt solutions at temperatures from 273 K to 363 K. *AIChE J*, 42:298–300, 2014. doi: https://doi.org/10.1002/aic.690420130. URL `https://aiche.onlinelibrary.wiley.com/doi/epdf/10.1002/aic.690420130`.

[43] Wolfram Böttinger, Michael Maiwald, and Hans Hasse. Online NMR spectroscopic study of species distribution in MEA–H2O–CO2 and DEA–H2O–CO2. *Fluid Phase Equilibria*, 263 (2):131–143, 2008. ISSN 0378-3812. doi: https://doi.org/10.1016/j.fluid.2007.09.017. URL `https://www.sciencedirect.com/science/article/pii/S037838120700605X`.

[44] Wei Xing, Min Yin, Qing Lv, Yang Hu, Changpeng Liu, and Jiujun Zhang. 1 - Oxygen Solubility, Diffusion Coefficient, and Solution Viscosity. In Wei Xing, Geping Yin, and Jiujun Zhang, editors, *Rotating Electrode Methods and Oxygen Reduction Electrocatalysts*, pages 1–31. Elsevier, Amsterdam, 2014. ISBN 978-0-444-63278-4. doi: https://doi.org/10.1016/B978-0-444-63278-4.00001-X. URL `https://www.sciencedirect.com/science/article/pii/B978044463278400001X`.

[45] Lucas Braakhuis and Hanna Knuutila. In *Modelling and Evaluating Carbamate Polymerization of Monoethanolamine in Post-Combustion Carbon Capture*. Trondheim Carbon Capture & Storage Conference, June 2021.

[46] Nikolett Sipöcz, Andrew Tobiesen, and Mohsen Assadi. Integrated modelling and simulation of a 400 MW NGCC power plant with CO2 capture. *Energy Procedia*, 4:1941–1948, 2011. ISSN 1876-6102. doi: https://doi.org/10.1016/j.egypro.2011.02.074. URL `https://www.sciencedirect.com/science/article/pii/S1876610211002712`. 10th International Conference on Greenhouse Gas Control Technologies.

[47] Jean-Marc G. Amann and Chakib Bouallou. CO2 capture from power stations running with natural gas (NGCC) and pulverized coal (PC): Assessment of a new chemical solvent based on aqueous solutions of N-methyldiethanolamine + triethylene tetramine. *Energy Procedia*, 1(1):909–916, 2009. ISSN 1876-6102. doi: https://doi.org/10.1016/j.egypro.2009.01.121. URL `https://www.sciencedirect.com/science/article/pii/S1876610209001222`. Greenhouse Gas Control Technologies 9.

[48] Oddvar Gorset, Jacob Nygaard Knudsen, Otto Morten Bade, and Inga Askestad. Results from Testing of Aker Solutions Advanced Amine Solvents at CO2 Technology Centre Mongstad. *Energy Procedia*, 63:6267–6280, 2014. ISSN 1876-6102. doi: https://doi.org/10.1016/j.egypro.2014.11.658. URL `https://www.sciencedirect.com/science/article/pii/S1876610214024734`. 12th International Conference on Greenhouse Gas Control Technologies, GHGT-12.

[49] Thor Mejdell, Terje Vassbotn, Olav Juliussen, Andrew Tobiesen, Aslak Einbu, Hanna Knuutila, Karl Anders Hoff, Vibeke Andersson, and Hallvard F. Svendsen. Novel full height pilot plant for solvent development and model validation. *Energy Procedia*, 4:1753–1760, 2011. ISSN 1876-6102. doi: https://doi.org/10.1016/j.egypro.2011.02.050. URL `https://www.sciencedirect.com/science/article/pii/S1876610211002475`. 10th International Conference on Greenhouse Gas Control Technologies.

[50] Park and Øi. Optimization of Gas Velocity and Pressure Drop in CO2 Absorption Column. Proceedings of the 58th SIMS, 2017. URL `http://dx.doi.org/10.3384/ecp17138292`.

[51] Viktor Andersson, Per Åke Franck, and Thore Berntsson. Temperature Dependence of Heat Integration Possibilities of an MEA Scrubber Plant at a Refinery. *Energy Procedia*, 37: 7205–7213, 2013. ISSN 1876-6102. doi: https://doi.org/10.1016/j.egypro.2013.06.658. URL `https://www.sciencedirect.com/science/article/pii/S1876610213009016`. GHGT-11 Proceedings of the 11th International Conference on Greenhouse Gas Control Technologies, 18-22 November 2012, Kyoto, Japan.

[52] Teeradet Supap, Raphael Idem, Amornvadee Veawab, Adisorn Aroonwilas, Paitoon Tontiwachwuthikul, Amit Chakma, and Brian D. Kybett. Kinetics of the Oxidative Degradation of Aqueous Monoethanolamine in a Flue Gas Treating Unit. *Industrial & Engineering Chemistry Research*, 40(16):3445–3450, 2001. doi: 10.1021/ie000957a. URL `https://doi.org/10.1021/ie000957a`.

[53] P.C. Rooney and D.D. Daniels. Oxygen solubility in various alkanolamine/water mixtures. *Petroleum Technology Quarterly*, pages 97–102, 1998.

[54] Hallvard F. Svendsen, Erik T. Hessen, and Thor Mejdell. Carbon dioxide capture by absorption, challenges and possibilities. *Chemical Engineering Journal*, 171(3):718–724, 2011. ISSN 1385-8947. doi: https://doi.org/10.1016/j.cej.2011.01.014. URL `https://www.sciencedirect.com/science/article/pii/S1385894711000416`. Special Section: Symposium on Post-Combustion Carbon Dioxide Capture.

[55] Camille Gouedard. *Novel degradation products of ethanolamine (MEA) in CO2 capture conditions : identification, mechanisms proposal and transposition to other amines*. Theses, Université Pierre et Marie Curie - Paris VI, September 2014. URL `https://tel.archives-ouvertes.fr/tel-01081315`.

[56] Grégoire Léonard, Dominique Toye, and Georges Heyen. Experimental study and kinetic model of monoethanolamine oxidative and thermal degradation for post-combustion CO2 capture. *International Journal of Greenhouse Gas Control*, 30:171–178, 2014. ISSN 1750-5836. doi: https://doi.org/10.1016/j.ijggc.2014.09.014. URL `https://www.sciencedirect.com/science/article/pii/S1750583614002758`.

APPENDIX A

APPENDIX

A.1 Fitted Parameters in the Advanced Model

Table A.1: Pre-exponential factors and activation energies for the reactions in the advanced oxidative degradation model.

Pre-exponential factor	Value	Activation energy	Value [J/mol]
A_1	$3.35 \cdot 10^{22}$ m^3/kmol day^{-1} (m^3/kmol)	Ea_1	$1.35 \cdot 10^5$
A_2	$5.20 \cdot 10^3$ m^3/kmol day^{-1}	Ea_2	$3.06 \cdot 10^4$
A_3	$4.66 \cdot 10^4$ m^3/kmol day^{-1}	Ea_3	$7.33 \cdot 10^3$
A_4	$7.17 \cdot 10^{10}$ day^{-1}	Ea_4	$4.60 \cdot 10^4$
A_5	$2.85 \cdot 10^{23}$ m^3/kmol day^{-1} (m^3/kmol)	Ea_5	$1.51 \cdot 10^5$
A_6	$5.23 \cdot 10^8$ m^3/kmol day^{-1} (m^3/kmol)^2	Ea_6	$3.83 \cdot 10^3$
A_7	$5.95 \cdot 10^{26}$ day^{-1}	Ea_7	$1.86 \cdot 10^5$
A_8	$7.91 \cdot 10^{12}$ m^3/kmol day^{-1}	Ea_8	$7.11 \cdot 10^4$
A_9	$8.27 \cdot 10^{21}$ m^3/kmol day^{-1}	Ea_9	$1.45 \cdot 10^5$
A_{10}	$1.42 \cdot 10^{26}$ day^{-1}	Ea_{10}	$1.59 \cdot 10^5$
A_{11}	$6.99 \cdot 10^{14}$ m^3/kmol day^{-1} (m^3/kmol)	Ea_{11}	$1.15 \cdot 10^5$

Table A.2: Reference reaction rate coefficient factors and activation energies for the reactions in the advanced thermal degradation model.

Reference reaction rate coefficient	Value	Activation energy	Value [J/mol]
k_{r1}	$7.23 \cdot 10^{-8}$ s^{-1}	Ea_1	$1.30 \cdot 10^5$
k_{r2}	$3.87 \cdot 10^{-10}$ m^3/mol s^{-1}	Ea_2	$1.00 \cdot 10^5$
k_{r3}	$1.35 \cdot 10^{-10}$ m^3/mol s^{-1}	Ea_3	$1.41 \cdot 10^5$
k_{r4}	$2.83 \cdot 10^{-10}$ m^3/mol s^{-1}	Ea_4	$1.71 \cdot 10^5$

A.2 Solvent Degradation Rig

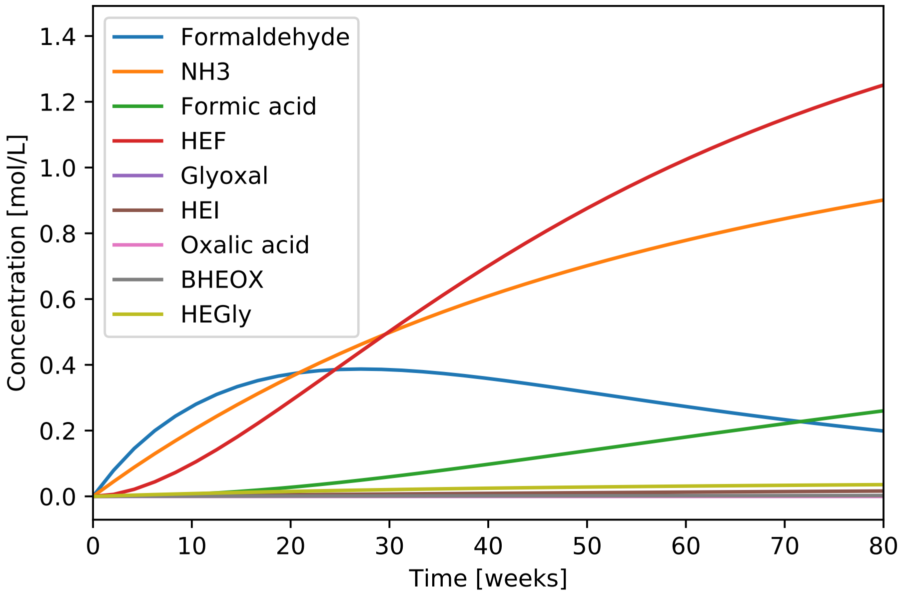

Figure A.1: Oxidative degradation compounds after 80 weeks at the SDR campaign.

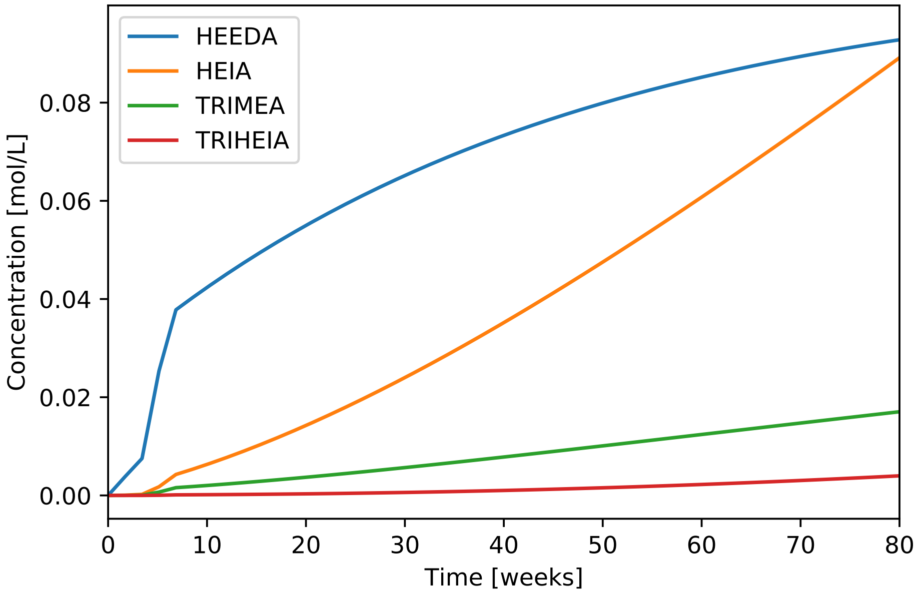

Figure A.2: Thermal degradation compounds after 80 weeks at the SDR campaign.

A.3 Calculations

$$3mgMEA/m^3 \cdot 1150m^3/h \cdot 4000h = 1.38 \cdot 10^7 mgMEA = 13.8kgMEA \tag{A.1}$$

$$kgMEA = \Delta C_{MEA} \cdot V \cdot MW_{MEA} = 3.21mol/L \cdot 3737 \cdot 10^3 L \cdot 61.08g/mol/1000g/kg = 732733kgMEA \tag{A.2}$$

A.4 Industrial Cases

Table A.3: Flue gas flow rate, pressure in absorber and desorber, temperature of flue gas and in the condenser and flue gas composition for the two industrial cases[11][46][47].

	Coal	Natural Gas
Flue gas flow rate [kmole/h]	54633	81867
Flue gas flow rate [Sm^3/s]	340	509
Absorber pressure [bar]	1.0	1.0
Desorber pressure [bar]	2.0	2.0
Temperature of flue gas [°C]	40	40
Temperature in condenser [°C]	20	20
Gas composition		
N_2[mol%]	70.9	74.3
CO_2[mol%]	14.6	5.0
O_2[mol%]	2.8	9.7
H_2O[mol%]	11.7	11.0
Dimensions		
Absorber height [m]	20.0	20.0
Absorber diameter [m]	14.7	18.0
Desorber height [m]	13.7	13.7
Desorber diameter [m]	11.8	14.4

Table A.4: Simulation results of the coal study, showing the different L/G ratios with respective lean and rich loading, reboiler duty, the specific energy consumption per ton CO_2 captured, and reboiler temperature.

Run	L/G	Reboiler Duty [MW]	Lean Loading	Rich Loading	GJ/ton CO_2, stripped	Reboiler Temperature [°C]
1	2.0	716	0.065	0.531	8.34	126
2	2.2	388	0.108	0.528	4.41	124
3	2.3	325	0.125	0.526	3.70	124
4	2.4	287	0.147	0.525	3.28	124
5	2.5	286	0.157	0.524	3.26	123
6	2.6	286	0.170	0.522	3.26	123
7	2.7	288	0.182	0.521	3.28	123
8	2.8	288	0.192	0.519	3.29	123
9	2.9	289	0.201	0.518	3.30	123
10	3.0	289	0.213	0.516	3.30	122
11	3.1	292	0.218	0.514	3.33	122
12	3.2	294	0.226	0.512	3.35	122
13	3.3	295	0.231	0.509	3.36	122
14	3.4	297	0.237	0.507	3.38	121
15	3.6	300	0.250	0.503	3.42	121
16	3.8	303	0.254	0.498	3.47	120
17	4.4	320	0.271	0.481	3.65	120
18	5.0	340	0.279	0.466	3.88	119
19	5.2	342	0.286	0.465	3.90	119
20	6.0	334	0.322	0.479	3.81	116
21	6.5	328	0.343	0.488	3.75	114
22	7.0	328	0.360	0.494	3.74	113

Table A.5: Simulation results of the NG study, showing the different L/G ratios with respective lean and rich loading, reboiler duty, the specific energy consumption per ton CO_2 captured, and reboiler temperature.

Run	L/G	Reboiler Duty [MW]	Lean Loading	Rich Loading	GJ/ton CO_2, stripped	Reboiler Temperature [°C]
1	0.75	400	0.064	0.505	9.00	125
2	0.80	231	0.100	0.505	5.19	124
3	0.90	154	0.146	0.505	3.45	123
4	1.00	152	0.181	0.504	3.41	123
5	1.10	152	0.205	0.504	3.41	122
6	1.20	152	0.230	0.503	3.42	121
7	1.30	153	0.246	0.501	3.42	121
8	1.40	153	0.262	0.499	3.44	120
9	1.50	156	0.275	0.495	3.47	119
10	1.60	158	0.284	0.491	3.54	119
11	1.70	161	0.290	0.486	3.59	118
12	2.00	177	0.295	0.463	3.95	118
13	2.20	183	0.302	0.454	4.09	118
14	2.50	195	0.303	0.438	4.36	117
15	3.00	209	0.315	0.427	4.68	117
16	3.50	210	0.329	0.437	4.68	115
17	4.00	216	0.350	0.438	4.83	113

Table A.6: Calculated solvent volumes in the industrial cases.

Case study	Absorption rate [kg_{CO_2}/h]	Specific volume $L/kg_{CO_2}h^{-1}$	Volume [L]
Coal	311430	12	3737160
NG	158566	12	1902792

A.5 Python Code

A.5.1 Oxygen Solubility Model by Weisenberger and Schumpe

```python
#!/usr/bin/env python3
# -*- coding: utf-8 -*-
"""
Created on Fri Jan 22 12:43:56 2021

@author: oyvindlille-maehlum
"""

import math
from scipy.interpolate import LinearNDInterpolator
import numpy as np

#The ion concentrations, "expData" were determined by Bottinger et al. (2008)

#Ion-concentration [MEAH+, MEACOO-, HCO3-]
expData = np.array([[0, 0, 0], [0.38, 0.38, 0], [0.75, 0.75, 0], [1.17, 1.17, 0], [1.53, 1.53, 0], [1.89, 1.89, 0], [2.18, 2.18, 0],
          [0.008, 0, 0], [0.63, 0.63, 0], [1.04, 1.04, 0], [1.18, 1.18, 0], [1.41, 1.41, 0], [1.71, 1.71, 0],[1.77, 1.77,0], [2.14, 2.14, 0], [2.33, 2.16, 0.17], [2.42, 2.20, 0.22],[2.49, 2.09, 0.39],
          [0, 0, 0], [0.64, 0.64, 0], [1.00, 1.00, 0], [1.31, 1.31, 0], [1.99, 1.80, 0.18], [2.16, 1.85, 0.31],
          [0, 0, 0], [0.29, 0.29, 0], [0.60, 0.60, 0], [0.96, 0.96, 0], [1.43, 1.43, 0], [1.62, 1.43, 0.20], [2.75, 2.07, 0.68]])

#Temperatures [K]
x = np.array([293.15, 293.15, 293.15, 293.15, 293.15, 293.15, 293.15,
             313.15, 313.15, 313.15, 313.15, 313.15, 313.15, 313.15, 313.15, 313.15, 313.15, 313.15,
             333.15, 333.15, 333.15, 333.15, 333.15, 333.15,
```

```
             353.15, 353.15, 353.15, 353.15, 353.15, 353.15, 353.15])

#Loading
y = np.array([0.0, 0.075, 0.15, 0.235, 0.309, 0.388, 0.474,
              0.0, 0.13, 0.21, 0.24, 0.28, 0.34, 0.35, 0.46, 0.47, 0.49, 0.51,
              0.0, 0.13, 0.20, 0.28, 0.42, 0.49,
              0.0, 0.06, 0.14, 0.25, 0.34, 0.40, 0.51])

#Interpolate to ion concentration based on loading and temperature
my_interpolating = LinearNDInterpolator((x, y), expData)

#Solubility of O2 in pure water, equation by Xing et al. (2014)
def O2solubility(T, p_o2):
      o2sol = (55.56*p_o2)/(math.e**(3.71814 + (5596.17/T) - (1049668/T**2))-p_o2)
      return o2sol #mol/L

h_meah   = 0.0133       #m3kmol^-1          ion-specific parameter (Buvik et al. 2020)
h_meacoo = 0.1284       #m3kmol^-1          ion-specific parameter (Buvik et al. 2020)
h_hco3   = 0.0967       #m3kmol^-1          ion-specific parameter (Buvik et al. 2020)
h_G0_o2  = 0            #m3kmol^-1          gas-specific parameter (Buvik et al. 2020)
h_T_o2   = -0.000334    #m3kmol^-1 K^-1     gas specific parameter (temperature dependency) (Buvik et al. 2020)
T_ref    = 298.15       #K


def o2inloadedmea(myTemp, myAlpha, p_o2):
    ion_cons = my_interpolating(myTemp, myAlpha)
    h_G_o2 = (h_G0_o2+h_T_o2)*(myTemp-T_ref)
    c_G_0 = O2solubility(myTemp, p_o2)
    logC0_logC = (h_meah+h_G_o2)*ion_cons[0] + (h_meacoo+h_G_o2)*ion_cons[1] + (h_hco3+h_G_o2)*ion_cons[2]
    C0_C = 10**(logC0_logC)
```

```

    return c_G_O/CO_C   #Dissolved O2 in MEA (temperature = myTemp,
    loading = myAlpha, partial pressure O2 = p_o2 [bar])
```

Listing A.1: Oxygen solubility model by Weisenberger and Schumpe (1996).

A.5.2 Rooney's Oxygen Solubility Model

```python
#!/usr/bin/env python3
# -*- coding: utf-8 -*-
"""
Created on Tue May 25 10:59:48 2021

@author: oyvindlille-maehlum
"""

import math
ppO2 = 0.12
rholiq = 1090.8
MWO2 = 32
P = 1.0
def RooneyO2(myTemp, myO2InFlueGas):
    x1 = 1/math.exp(3.71814 + (5596.17/myTemp) -(1049668/(myTemp**2)))
    ppm1 = x1*(32/18)*1000000*ppO2
    C1 = ppm1*rholiq*10**(-6)/MWO2
    H = ppO2*P/C1
    C_O2 = myO2InFlueGas*P/H
    return C_O2
```

Listing A.2: Oxygen solubility model by Rooney (1998).

A.5.3 Optimisation of Equation

```
"""
Created on Wed Feb 24 12:52:35 2021

@author: Oyvind Lille-Maehlum, Lucas Braakhuis
"""
import matplotlib.pyplot as plt
from scipy.optimize import minimize
import numpy as np
import math

# The degradation model
def deg_fun(b,X):
    y0,t,T,co2 = X.T
    R = 8.314        #Gas constant
    A  = 10**b[0]    #Pre-exponential factor
    EA = 10**b[1]    #Activation energy
    n = b[2]         #Reaction order of O2

    kr = A * np.exp(-EA/(R*T))
    R  = kr*(co2**(n))#*y0**(s)
    yt = y0-R*t
    return yt

# The objective function to minimize by the optimization
def obj_fun(b,*args):
    X,Y  = args
    yhat = deg_fun(b,X)
    eps  = yhat-Y
    RSS  = np.sum(eps**2)
    #print(RSS)
    return RSS


## Fitting the objective function
#Y:     Each row contains 5 intervals for each experiment. These
    are concentration [mol/L] of MEA after "time" seconds.
Y = np.array([5.33, 5.03, 4.93, 4.59, 4.49,
```

```
              4.94, 4.79, 4.72,  4.48, 4.17,
              4.62, 4.55, 4.44, 4.26, 4.03,
              4.86, 4.71, 4.67, 4.42, 4.05,
              4.66, 4.52, 4.37, 4.04, 3.72,
              4.00, 3.58, 3.37, 2.69, 2.36,
              4.95, 4.72, 4.79, 4.43, 3.47,
              4.68, 4.16, 3.42, 2.72, 1.95,
              4.17, 3.44, 3.14, 2.06, 1.58])

#y0:    Each row contains 5 intervals for each experiment. These are initial concentration [mol/L] of MEA.
y0   = np.array([5.46, 5.33, 5.03, 4.93, 4.66,
                 5.02, 4.9, 4.79, 4.64, 4.35,
                 4.91, 4.62, 4.51, 4.44, 4.26,
                 4.91, 4.86, 4.96, 4.67, 4.46,
                 4.78, 4.66, 4.52, 4.21, 3.86,
                 4.48, 4.00, 3.58, 3.37, 2.69,
                 5.28, 4.95, 4.91, 4.79, 3.78,
                 4.94, 4.68, 3.77, 2.99, 2.24,
                 5.43, 4.17, 3.44, 3.16, 2.06])

#time:  Seconds per interval
time = np.array([345600, 604800, 604800, 604800, 604800,
                 86400, 172800, 172800, 259200, 345600,
                 172800, 86400, 259200, 345600, 604800,
                 172800, 345600, 604800, 604800, 604800,
                 86400, 172800, 172800, 259200, 345600,
                 345600, 259200, 345600, 604800, 604800,
                 172800, 259200, 172800, 259200, 518400,
                 86400, 172800, 172800, 172800, 259200,
                 172800, 345600, 259200, 604800, 604800])

#T:     Temperature of the solution for each interval
T = np.array([328.15, 328.15, 328.15, 328.15, 328.15,
             328.15, 328.15, 328.15, 328.15, 328.15,
             328.15, 328.15, 328.15, 328.15, 328.15,
             338.15, 338.15, 338.15, 338.15, 338.15,
             338.15, 338.15, 338.15, 338.15, 338.15,
             338.15, 338.15, 338.15, 338.15, 338.15,
```

```
             348.15, 348.15, 348.15, 348.15, 348.15,
             348.15, 348.15, 348.15, 348.15, 348.15,
             348.15, 348.15, 348.15, 348.15, 348.15])

#co2:  Oxygen solubility [mol/L] for each interval. These were calculated by o2sol.py, by the Schumpe model.
co2 = np.array([0.0000265756, 0.0000265756, 0.0000265756, 0.0000265756, 0.0000265756,
                0.000110017, 0.000110017, 0.000110017, 0.000110017, 0.000110017,
                0.000256709, 0.000256709, 0.000256709, 0.000256709, 0.000256709,
                0.0000258572, 0.0000258572, 0.0000258572, 0.0000258572, 0.0000258572,
                0.000107041, 0.000107041, 0.000107041, 0.000107041, 0.000107041,
                0.000249764, 0.000249764, 0.000249764, 0.000249764, 0.000249764,
                0.0000278957, 0.0000278957, 0.0000278957, 0.0000278957, 0.0000278957,
                0.00011548, 0.00011548, 0.00011548, 0.00011548, 0.00011548,
                0.000269456, 0.000269456, 0.000269456, 0.000269456, 0.000269456])
X    = np.column_stack((y0,time,T,co2))


b0  = [2.88,4.7652, 0.24] # Initial guess for A, Ea and n
sol = minimize(obj_fun,b0,method='Nelder-Mead',args=(X,Y))

bopt = sol.x

print(sol)
print(bopt)
print(10**bopt)


#Evaluating and plotting
yhat = deg_fun(bopt,X)
```

```python

plt.xlabel('Time [s]')
plt.ylabel('MEA Concentration [mol/L]')
plt.plot(X[:,1],Y,'bx')
plt.plot(X[:,1],yhat,'r.')
print(obj_fun(b0, X,Y))
```

Listing A.3: Nelder-Mead method to optimise the parameters in the simplified oxidative degradation equation.

A.5.4 Simple Degradation Model

```
#!/usr/bin/env python3
# -*- coding: utf-8 -*-
"""
Created on Thu May 13 15:28:40 2021

@author: oyvindlille-maehlum
"""
#Simplified model for MEA consumption, only
import numpy as np
import math
from scipy.integrate import odeint
import matplotlib.pyplot as plt
from o2sol import o2inloadedmea
R = 8.314                        #J/K mol
V = 3000                         #L
T_desorber = 393.15              #K
T_absorber = 313.15              #K
Tr = 400                         #K, reference temperature for the thermal degradation
a_rich = 0.50                    #Rich loading [mol CO2/mol MEA]
a_lean = 0.2                     #Lean loading [mol CO2/mol MEA]
o2_in_fluegas = 0.05             #mol%
o2sol = o2inloadedmea(T_absorber, a_rich, o2_in_fluegas) #oxygen solubility calculated by the Schumpe model
Cnox = 130                       #ppm
Csox = 1                         #ppm
flow_rate = 1150                 #Sm3/h
y0 = 4.911                       #mol/L, initial MEA concentration
t = np.linspace(0, 14400000)     #[s] Duration of model

def co2sol(loading, MEA):
    return loading*MEA          #mol/L

def func_thermal(T_desorber):
    #From a in-house model
    kr = 3.34*10**(-11)
    Ea = 1.39*10**(5)
```

```python
    return kr*math.e**((-Ea/R)*((1/(T_desorber)) - (1/Tr)))

def func_oxidative(o2sol, T_absorber):
    #Parameters found by Nelder-Mead on oxidative study by
   Vevelstad et al. (2014)
    E0 = 10**(4.71760454)   #Activation energy
    A =   10**(2.88018259)  #Pre-exponential factor
    n = 0.23618788          #Reaction order of O2
    rmea_oxidative= A*math.e**(-E0/(R*T_absorber))*(o2sol**(n)) #
   mol/Ls
    return rmea_oxidative


def func_NOx(flow_rate, Cnox):
    #Concentration of NOx is multiplied with 5%, as 5% is NO2
    #Flowrate is multiplied with 1000L/m3 and is divided by 60min/h
   , 60 s/min and 22.4 L/mol
    return (Cnox*0.05/1000000)*(flow_rate*1000/(60*60*22.4))*0.25*2
    #mol MEA/s

def func_SOx(flow_rate, Csox):
    #Flowrate is multiplied with 1000L/m3 and is divided by 60min/h
   , 60 s/min and 22.4 L/mol
    return (Csox/1000000)*(flow_rate*1000/(60*60*22.4))*0.995*2  #
   mol MEA/s

def model(y, t):

    #Rate of reactions
    #Desorber packing, sump and reboiler
    R1 = np.zeros(1)
    #Hot rich piping
    R2 = np.zeros(1)
    #Hot lean piping and HEX
    R3 = np.zeros(1)

    #For oxidative (R[0]) and impurities (R[1])
    R = np.zeros(2)

```

```python
    #Rate constats
    #Desorber packing, sump and reboiler
    k1 = np.zeros(1)
    #Hot rich piping
    k2 = np.zeros(1)
    #Hot lean piping and HEX
    k3 = np.zeros(1)

    for i in range(1):
            #Volume1, a = 0.2
            k1[i] = (func_thermal(T_desorber))
            #Volume2, a = 0.5, temperature assumed 10 degrees lower
            #in hot rich piping
            k2[i] = (func_thermal(T_desorber -10))
            #Volume3, a = 0.2, temperature assumed 10 degrees lower
            #in lean rich piping and HEX
            k3[i] = (func_thermal(T_desorber -10))


    #The rate of reactions for thermal degradation below is
    #multiplied with 1000 because it is based on concentrations
    #of mol/m3 for MEA and CO2, and input concentration has [mol/L].
    #Further, divided by 1000 such that Ri [mol/m3s]--> mol/Ls
    #R1: Rate of reactions in the desorber packing, sump and reboiler.
    R1[0] = (k1[0]*y[0]*co2sol(a_lean, y[0]))*1000
    #R2: Rate of reactions in hot rich piping.
    R2[0] = (k2[0]*y[0]*co2sol(a_rich, y[0]))*1000
    #R3: Rate of reactions in lean rich piping and HEX.
    R3[0] = (k3[0]*y[0]*co2sol(a_lean, y[0]))*1000


    #Oxidative
    R[0] = func_oxidative(o2sol, T_absorber)
    #Impurities
    R[1] = func_NOx(flow_rate, Cnox) +  func_SOx(flow_rate, Csox)


```

```


    #####Volumes for the SDR#####
    #Volume exposed to oxidative degradation
    #V_oxidative = 0.44*V*(6/16)+0.60*V*(10/16)     #L
    #Volume exposed to thermal degradation in desorber packing, sump and reboiler.
    #V_thermal1 = 0.095*V*(6/16)
    #Volume exposed to thermal degradation in hot rich piping.
    #V_thermal2 = 0.029*V*(6/16) #L
    #Volume exposed to thermal degradation in hot lean piping and HEX.
    #V_thermal3 = 0.229*V*(6/16) #L


    #####Volumes for base case and pilot plant#####
    #Volume exposed to oxidative degradation
    V_oxidative = 0.44*V  #L
    #Volume exposed to thermal degradation in desorber packing, sump and reboiler.
    V_thermal1= 0.095*V   #L
    #Volume exposed to thermal degradation in hot rich piping.
    V_thermal2 = 0.029*V  #L
    #Volume exposed to thermal degradation in hot lean piping and HEX.
    V_thermal3 = 0.229*V  #L

    #Returns new MEA concentration
    dydt = [#Thermal
        (-(R1[0]*V_thermal1) -(R2[0]*V_thermal2) -(R3[0]*V_thermal3)
            #Oxidative
              -(R[0]*V_oxidative)
            #Impurities
              - R[1])/V]
    return dydt

y = odeint(model, y0, t)

```

```
plt.plot(t/(3600*24*7),y[:,0], label = "Simplified model")
plt.legend(loc=2, prop={'size': 8})
plt.legend()
plt.xlabel('Time [weeks]')
plt.ylabel('[MEA] [mol/L]')
axes = plt.gca()
plt.show()
```

Listing A.4: The simplified model in Python.

A.5.5 Advanced Degradation Model

```
#!/usr/bin/env python3
# -*- coding: utf-8 -*-
"""
Created on Fri May 14 11:16:14 2021

@author: oyvindlille-maehlum
"""

import numpy as np
import math
from scipy.integrate import odeint
import matplotlib.pyplot as plt
from Rooney import RooneyO2

R             = 8.314      #J/K mol
T_absorber    = 336.55     #K
T_desorber    = 396.15     #K
Tr            = 400        #K, reference temperature for thermal model
O2_fluegas    = 0.028      #mol% O2 in flue gas,
V             = 4.0909     #L, total solvent volume
a_rich        = 0.500      #mol CO2/mol MEA
a_lean        = 0.200      #mol CO2/mol MEA
Nox_inFlueGas = 10         #ppm
Sox_inFlueGas = 1          #ppm
flowrate      = 1*60/1000  #Sm3/h
COMEA         = 6.787      #mol/L
COH2O         = 38         #mol/L
o2sol         = RooneyO2(T_absorber, O2_fluegas) #Oxygen solubility calculated from the oxygen solubility model by Rooney (1998)
####Change time if the model does not converge####
time          = 159         #Run time [days] If the model doesn't converge, change this variable, and adjust plots with x_lim.

                #####Volumes for the SDR#####
#Volume exposed to oxidative degradation
#V_oxidative = 0.44*V*(6/16)+0.60*V*(10/16)     #L
```

```
#Volume exposed to thermal degradation in desorber packing, sump and reboiler.
#V_thermal1 = 0.095*V*(6/16)
#Volume exposed to thermal degradation in hot rich piping.
#V_thermal2 = 0.029*V*(6/16) #L
#Volume exposed to thermal degradation in hot lean piping and HEX.
#V_thermal3 = 0.229*V*(6/16) #L


                #####Volumes for base case and pilot plant#####
#Volume exposed to oxidative degradation
V_absorber = 0.44*V  #L
#Volume exposed to thermal degradation in desorber packing, sump and reboiler.
V_thermal1= 0.095*V   #L
#Volume exposed to thermal degradation in hot rich piping.
V_thermal2 = 0.029*V  #L
#Volume exposed to thermal degradation in hot lean piping and HEX.
V_thermal3 = 0.229*V  #L

#Thermal degradation equation
def func(kr, Ea, T, t):
    return kr*math.e**((-Ea/R)*((1/(T)) - (1/Tr)))

#Degradation from NOx
def funcnox(Nox_inFlueGas, flowrate):
    return (Nox_inFlueGas*0.05/1000000)*(flowrate*1000)/(60*60*22.4)*0.25*2

#Degradation from SOx
def funcsox(Sox_inFlueGas, flowrate):
    return (Sox_inFlueGas/1000000)*(flowrate*1000)/(60*60*22.4)*0.995*2

def model(y, t):
    ###Degradation from impurities
    #Mol/s MEA degraded from NOx
    NOxDegradation = funcnox(Nox_inFlueGas, flowrate)
    #Mol/s MEA degraded from SOx
```

```
    SOxDegradation = funcsox(Sox_inFlueGas, flowrate)

    #Lists of R_O and kr for oxidative degradation
    R_O = np.zeros(8)       #Rate of reaction
    kr = np.zeros(11)       #Reaction constants

                            #Oxidative degradation
                #Pre-exponential factor and activation energy
                            #UNITS: See Table A.1
    A   = [3.35*10**(22),   #A1
          5.20*10**(3),     #A2
          4.66*10**(4),     #A3
          7.17*10**(10),    #A-3
          2.85*10**(23),    #A4
          5.23*10**(8),     #A5
          5.95*10**(26),    #A-5
          7.91*10**(12),    #A6
          8.27*10**(21),    #A7
          1.42*10**(26),    #A-7
          6.99*10**(14)]    #A8

                            #UNIT [J/mol]
    Ea = [1.35*10**(5),     #Ea1
          3.06*10**(4),     #Ea2
          7.33*10**(3),     #Ea3
          4.60*10**(4),     #Ea-3
          1.51*10**(5),     #Ea4
          3.83*10**(3),     #Ea5
          1.86*10**(5),     #Ea-5
          7.11*10**(4),     #Ea6
          1.45*10**(5),     #Ea7
          1.59*10**(5),     #Ea-7
          1.15*10**(5)]     #Ea8

    #Reaction rates for the oxidative degradation reactions
    kr[0] = A[0]*math.e**(-Ea[0]/(R*T_absorber))
    kr[1] = A[1]*math.e**(-Ea[1]/(R*T_absorber))
    kr[2] = A[2]*math.e**(-Ea[2]/(R*T_absorber))
    kr[3] = A[3]*math.e**(-Ea[3]/(R*T_absorber))
```

```
    kr[4] = A[4]*math.e**(-Ea[4]/(R*T_absorber))
    kr[5] = A[5]*math.e**(-Ea[5]/(R*T_absorber))
    kr[6] = A[6]*math.e**(-Ea[6]/(R*T_absorber))
    kr[7] = A[7]*math.e**(-Ea[7]/(R*T_absorber))
    kr[8] = A[8]*math.e**(-Ea[8]/(R*T_absorber))
    kr[9] = A[9]*math.e**(-Ea[9]/(R*T_absorber))
    kr[10] = A[10]*math.e**(-Ea[10]/(R*T_absorber))


    #Thermal degradation
    #Divided into three parts as the loading and temperature varies
   .
    #Rate of reactions
    R_T1 = np.zeros(4)      #Desorber packing, sump and reboiler
    R_T2 = np.zeros(4)      #Hot rich piping
    R_T3 = np.zeros(4)      #Hot lean piping and HEX

    #Rate coefficients
    k_T1 = np.zeros(4)      #Desorber packing, sump and reboiler
    k_T2 = np.zeros(4)      #Hot rich piping
    k_T3 = np.zeros(4)      #Hot lean piping and HEX


    #Reaction rates, See table A.2 for units. These are multiplied
   with 86400 s/day to get a reaction rate per day
    kr_T = [7.23*10**(-8)*86400, 3.87*10**(-10)*86400,
   1.35*10**(-10)*86400, 2.83*10**(-10)*86400]
    #Activation energy [J/mol]
    Ea_T = [1.30*10**(5), 1.00*10**(5), 1.41*10**(5), 1.71*10**(5)]

    #Set the concentration low if they get unreasonable values
    for element in range(len(y)):
        if y[element]<0:
            y[element] = 1*10**(-19)
        if y[element]>10:
            y[element] = 1*10**(-19)

    #Rate of reacions, oxidative
    #These reactions are found in the Method Section describing
```

```
oxidative degradation in the advanced model
    #Units: [mol/Lday]
    R_O[0] = kr[0]*(a_rich**(2))*y[1]**(2.639)*(y[0]**(0.998))
    R_O[1] = kr[1]*(y[2])**(0.936)*(y[0]**(0.107))
    R_O[2] = kr[2]*((a_rich*y[1])**(0.657))*((y[4])**(0.649)) - kr[3]*((y[5])**(0.822))
    R_O[3] = kr[4]*(y[1]*a_rich**(2)**(0.598))*(y[0]**(0.785))
    R_O[4] = kr[5]*((y[1])**(0.754))*((y[2])**(0.290))*((y[3])**(0.961))*((y[7])**(1.169)) - kr[6]*((y[8])**(0.643))
    R_O[5] = kr[7]*((y[7])**(0.373))*(y[0]**(0.565))
    R_O[6] = kr[8]*((y[1]*a_rich)**(0.075))*((y[9])**(0.230)) - kr[9]*((y[10])**(1.093))
    R_O[7] = kr[10]*((a_rich**(2))*y[1]**(2.972))*(y[0]**(0.296))

    #Calculates reaction constants for the thermal degradation
    #Thermal degradation occur in three locations, which has been described, where the latter two have a temperature 10 degrees less than the stripping temperature.
    for i in range(len(kr_T)):
        k_T1[i] = (func(kr_T[i], Ea_T[i], T_desorber, t))
        k_T2[i] = (func(kr_T[i], Ea_T[i], T_desorber-10, t))
        k_T3[i] = (func(kr_T[i], Ea_T[i], T_desorber-10, t))

    #The CO2 concentration, y[12] is multiplied with a_lean/a_rich for the parts where it is assumed to be a lean loading. As the initial CO2 concentration was set to (a_rich * [MEA])

    #Rate of reactions, thermal
    #All concentrations y[i] are multiplied with 1000 to get unit [mol/m3]
    #All reactions are divided by 1000 in order to get unit [mol/L*day]
    ycar = min(y[12]*(a_lean/a_rich), y[1]/2)  #Min of CO2 concentration or MEA/2
    R_T1[0] = (k_T1[0]*ycar*1000)/(1000)
    R_T1[1] = (k_T1[1]*y[14]*1000*y[12]*(a_lean/a_rich)*1000)/(1000)
    R_T1[2] = (k_T1[2]*y[14]*1000*ycar*1000)/(1000)
    R_T1[3] = (k_T1[3]*y[16]*1000*y[12]*(a_lean/a_rich)*1000)
```

```
/(1000)

 ycar = min(y[12], y[1]/2)  #Min of CO2 concentration or MEA/2
 R_T2[0] = (k_T2[0]*ycar*1000)/(1000)
 R_T2[1] = (k_T2[1]*y[14]*1000*y[12]*1000)/(1000)
 R_T2[2] = (k_T2[2]*y[14]*1000*ycar*1000)/(1000)
 R_T2[3] = (k_T2[3]*y[16]*1000*y[12]*1000)/(1000)

 ycar = min(y[12]*(a_lean/a_rich), y[1]/2)  #Min of CO2 concentration or MEA/2
 R_T3[0] = (k_T3[0]*ycar*1000)/(1000)
 R_T3[1] = (k_T3[1]*y[14]*1000*y[12]*(a_lean/a_rich)*1000)/(1000)
 R_T3[2] = (k_T3[2]*y[14]*1000*ycar*1000)/(1000)
 R_T3[3] = (k_T3[3]*y[16]*1000*y[12]*(a_lean/a_rich)*1000)/(1000)

 dydt = [
     #O2
     0,
     #MEA_Oxidative
     ((-R_O[0] - R_O[2] - 2*R_O[3] -2*R_O[7] - R_O[4] - 2*R_O[6])*V_absorber +
     #MEA_Thermal
     (-2*R_T1[0]-R_T1[2])*V_thermal1  + (-2*R_T2[0]-R_T2[2])*V_thermal2 + (-2*R_T3[0]-R_T3[2])*V_thermal3
     #MEA_impurities
     #Multiplied with seconds per day
     -(NOxDegradation*3600*24 + SOxDegradation*3600*24))/V,
     #Formaldehyde
     (2*R_O[0] - R_O[1] - R_O[4])*V_absorber/V,
     #NH3
     (R_O[0]  + 2*R_O[3] + R_O[7] - R_O[4])*V_absorber/V,
     #Formic Acid/ Formate
     (R_O[1] - R_O[2])*V_absorber/V,
     #HEF
     R_O[2]*V_absorber/V,
     #H2O
     (R_O[2] + 2*R_O[3] + R_O[7] + 3*R_O[4] + 2*R_O[6])*
```

```
    V_absorber/V,
        #Glyoxal
        (2*R_O[3] - R_O[5] - R_O[4])*V_absorber/V,
        #HEI
        R_O[4]*V_absorber/V,
        #Oxalic acid
        (R_O[5] - R_O[6])*V_absorber/V,
        #BHEOX
        R_O[6]*V_absorber/V,
        #HEGly
        R_O[7]*V_absorber/V,
        #CO2
        ((-R_T1[1]-R_T1[3])*V_thermal1 +(-R_T2[1]-R_T2[3])*
    V_thermal2 +(-R_T3[1]-R_T3[3])*V_thermal3)/V,
        #OZD
        0,
        #HEEDA
        ((R_T1[0]-R_T1[1]-R_T1[2])*V_thermal1 + (R_T2[0]-R_T2[1]-
    R_T2[2])*V_thermal2 + (R_T3[0]-R_T3[1]-R_T3[2])*V_thermal3)/V,
        #HEIA
        (R_T1[1]*V_thermal1 + R_T2[1]*V_thermal2 + R_T3[1]*
    V_thermal3)/V,
        #TRIMEA
        ((R_T1[2]-R_T1[3])*V_thermal1 + (R_T2[2]-R_T2[3])*
    V_thermal2+ (R_T3[2]-R_T3[3])*V_thermal3)/V,
        #TRIHEIA
        (R_T1[3]*V_thermal1 + R_T2[3]*V_thermal2 +R_T3[3]*
    V_thermal3)/V,
        #AEHEIA
        0,
        #MEA Urea
        0]
    return dydt


t = np.linspace(0,time)

#Initial concentration of the compounds, dydt in function "model"
    to see which is which
```

```
y0 = [o2sol, COMEA, 0, 0, 0, 0, COH2O, 0, 0, 0, 0, 0, a_rich*COMEA,
     0, 0, 0 ,0 ,0 ,0, 0]
y = odeint(model, y0, t)

# plt.plot(t,y[:,0], label = "O2")
plt.plot(t/7,y[:,1], label = "MEA")
# plt.plot(t/7,y[:,2], label = "Formaldehyde")
# plt.plot(t/7,y[:,3], label = "NH3")
# plt.plot(t/7,y[:,4], label = "Formic acid")
# plt.plot(t/7,y[:,5], label = "HEF")
# plt.plot(t,y[:,6], label = "H2O")
# plt.plot(t/7,y[:,7], label = "Glyoxal")
# plt.plot(t/7,y[:,8], label = "HEI")
# plt.plot(t/7,y[:,9], label = "Oxalic acid")
# plt.plot(t/7,y[:,10], label = "BHEOX")
# plt.plot(t/7,y[:,11], label = "HEGly")
# plt.plot(t,y[:,12], label = "CO2")
# plt.plot(t/7,y[:,13], label = "OZD")
# plt.plot(t/7,y[:,14], label = "HEEDA")
# plt.plot(t/7,y[:,15], label = "HEIA")
# plt.plot(t/7,y[:,16], label = "TRIMEA")
# plt.plot(t/7,y[:,17], label = "TRIHEIA")
# plt.plot(t/7,y[:,18], label = "AEHEIA")
# plt.plot(t/7,y[:,19], label = "MEAUREA")

plt.legend(loc=2, prop={'size': 8})
plt.legend()
plt.xlabel('Time [weeks]')
plt.ylabel('[MEA] [mol/L]')
axes = plt.gca()
plt.show()
```

Listing A.5: The advanced model in Python.

Øyvind Vilfred Haugberg Lille-Mæhlum

Modelling Solvent Degradation in Amine-based Post-combustion Carbon Capture

NTNU
Norwegian University of
Science and Technology